UNIVERSITEIT VAN PRETORIA
UNIVERSITY OF PRETORIA
YUNIBESITHI YA PRETORIA

Bubbling to Turbulent Regime Transition in a 2D Catalytic Fluidized Bed Reactor

by

Jean Saayman

A dissertation submitted in partial fulfilment of
the requirements for the degree

Master of Engineering (Chemical Engineering)

in the

Department of Chemical Engineering

Faculty of Engineering, the Build Environment and Information Technology

University of Pretoria

11 December 2009

Bubbling to Turbulent Regime Transition in a 2D Catalytic Fluidized Bed Reactor

Author : Jean Saayman
Supervisor : W. Nicol
Department : Department of Chemical Engineering
University of Pretoria
Degree : Master of Engineering (Chemical Engineering)

Synopsis

The ozone decomposition reaction was performed in a 2.5cmx40cmx450cm two dimensional (2D) catalytic fluidized bed reactor. Commercial FCC catalyst impregnated with Fe_2O_3 was used at superficial gas velocities ranging between 0.006 m/s and 0.55 m/s. The onset velocity of the turbulent regime (u_c) was determined as 0.4 m/s. The catalyst activity was optimized so that the effect of inter-phase mass transfer could be accentuated in the conversion reading. It was found that the general bubbling-turbulent model of Thompson et. al. (1999) combined with the mass transfer correlations of Kunii and Levenspiel (1991), Foka et. al. (1996) and Miyauchi et. al. (1980) gave reasonable predictions of the experimental data. The gradual improvement of reactor performance with an increase in superficial velocity (as predicted by the Thompson et. al. model) was not observed; instead a discontinuity of the reactor performance was noted in the vicinity of u_c. More experimental work is required to substantiate this observation.

KEYWORDS: Two-Dimensional Fluidized Beds, Bubbling-Turbulent Reactor Models, Ozone decomposition reaction.

Contents

Nomenclature

a_I	-	Inter-phase transfer surface	[m^{-1}]
Ar	-	Archimedes number (= $d_p^3.\rho_g.(\rho_s-\rho_g).g/\mu^2$)	[-]
C_i	-	Gas concentration of species I	[$kmol/m^3$]
$C_{i,IN}$	-	Inlet concentration	[$kmol/m^3$]
D	-	Reactor diameter	[m]
D_m	-	Gas diffusion coefficient	[m^2/s]
d_b	-	Bubble diameter	[m]
d_p	-	Particle diameter	[m]
d_p^*	-	Modified particle diameter (=$Ar^{1/3}$)	[m]
D_z	-	Axial dispersion coefficient	[m^2/s]
f_{kq}	-	Coefficient in the Sit and Grace k_q correlation	[-]
F_P	-	Degree of pressure fluctuations	[-]
f_{Pe}	-	Coefficient in the Bi and Grace Pe correlation	[-]
g	-	Gravitational acceleration (9.81)	[m/s^2]
G_s	-	Solids circulation rate/ Entrainment rate	[$kg/s.m^2$]
H_b	-	Bed height	[m]
K_{BC}	-	Bubble-Cloud mass transfer	[s^{-1}]
K_{BE}	-	Bubble-Emulsion mass transfer	[s^{-1}]
K_{CE}	-	Cloud-Emulsion mass transfer	[s^{-1}]
k_q	-	Inter-phase mass transfer rate constant	[m/s]
$k_r^{```}$	-	Reaction rate constant based on volume catalyst	[s^{-1}]
P	-	Pressure at a single point	[Pa]
ΔP	-	Pressure drop	[Pa]
Pe	-	Peclet number ($U.H_b/D_z$)	[-]
q	-	Volumetric flow rate ratio (q_i/Q_{TOTAL})	[-]
Q	-	Volumetric flow rate	[m^3/s]
Re	-	Reynolds number ($d_p.u_o.\rho_g/\mu$)	[-]
Sc	-	Scmidt number ($\mu/(\rho_g.D_m)$)	[-]
u_b	-	Bubble velocity	[m/s]
u_{br}	-	Single bubble rise velocity	[m/s]
u_c	-	Minimum turbulent velocity 1	[m/s]

u_C	-	Cloud phase velocity	[m/s]
u_E	-	Emulsion phase velocity	[m/s]
u_k	-	Minimum turbulent velocity 2	[m/s]
u_{mb}	-	Minimum bubble velocity	[m/s]
u_{mf}	-	Minimum fluidization velocity	[m/s]
u_{mf}^*	-	Modified minimum fluidization velocity ($Re/Ar^{1/3}$)	[m/s]
u_o	-	Operating velocity	[m/s]
u_{se}	-	Significant entrainment velocity	[m/s]
u_{tr}	-	Transport velocity	[m/s]
z	-	Height in reactor (from distributor)	[m]

Subscripts

B	-	Bubble phase (Low density phase)
b	-	Bubble
C	-	Cloud phase
E	-	Emulsion phase (High density phase)
H	-	High density phase
L	-	Low density phase
mf	-	Minimum fluidization
$\bar{P}$	-	Average value

Greek letters

ε	-	Gas volume fraction	[-]
ρ	-	Bulk density	[kg/m^3]
ρ_s	-	Particle density	[kg/m^3]
ρ_g	-	Gas density	[kg/m^3]
μ	-	Gas viscosity	[Pa.s]
Φ	-	Solids volume fraction (1-ε)	[-]
$\Phi_{L,0}$	-	Solids volume fraction in the L-Phase in a bubble bed	[-]
ψ	-	Phase volume fraction	[-]

1 Introduction

Gas-Solid Fluidization entails the upward flow of gas through a bed of solid particles. At a high enough gas velocity the particles become suspended, and the bed of solids adopts fluid-like properties. In Catalytic Fluidized Bed Reactors (CFBR's) the reactant is in the gas phase and the catalyst is the solid phase. Due to numerous advantages compare to conventional packed bed reactors CFBR's are used extensively in the processing industry (Kunii & Levenspiel, 1991:10-11). The complex nature of gas-solid fluidization gives rise to different hydrodynamic regimes. These are mainly characterized by the superficial gas velocity. The low velocity regimes include the particulate-, bubbling- and slugging fluidization regimes and because of the low entrainment rates an internal solids return system is typically adequate to return the solids to the bed. Examples of such CFBR's are Fluid Catalytic Cracking (FCC) reactors (Kunii & Levenspiel, 1991:36) and High Temperature Fisher Tropsch (HTFT) reactors. At increased superficial velocities entrainment becomes more severe and this is typically accompanied by external removal and solids circulation of solids. The turbulent and fast fluidization regimes are encountered at these velocities. Commercial examples of CFBR's operating in these regimes are Zinc Sulphide Roasters, Mobil MTG-, Acrylonitrile-, Maleic Anhydride-, Phthalic Anhydride- and Ethylene Dichloride- reactors (Bi et. al. 2000: 4791).

Except for particulate fluidization, encounter for only certain solid types, most of the regimes are characterized by a lean gaseous phase and a dense phase, consisting mainly of solids. The structure and behaviour of these phases are different for each of the regimes, causing reactor performance to alter significantly for the different regimes. The prime reason for the performance differences lies in the inter-phase mass transfer where gaseous reactant has to be transported from the lean to the dense phase. In this regard numerous reaction studies have been performed (Fryer & Potter, 1976; Heidel et. Al., 1965; Massimilla & Johnstone, 1961 and Shen &

Johnstone, 1995) to quantify the effect of inter-phase mass transfer in a specific regime. However, fewer studies have focused on the regime transition boundary and the only prominent work in this regard is the work by Sun (1991) where the velocities ranged from bubbling fluidization up to fast fluidization. It was observed that the greatest change in reactor performance occurs during the bubbling to turbulent regime transition. This is very interesting since numerous commercial reactors operate in this regime transition.

The University of Pretoria's Reaction Engineering Research group is mainly sponsored by Sasol and the research focus is structured to further our understanding of fluidization, but also to benefit Sasol. Therefore one of the focus areas of the group is based on the Sasol Advanced Synthol (SAS) reactors, used for performing HTFT reactions. These reactors operate between the bubbling and turbulent regimes and use high density (approx. 6600 kg/m^3) catalyst that differs significantly from other commercial fluidization catalyst. Therefore scope exists for exploring the hydrodynamic properties of this catalyst using the insights and developments of research performed on lighter catalysts. In this regard reaction quantification in a CFBR was identified as a crucial hydrodynamic measurement tool and this specific project aims at building expertise with the use of this tool. Since this project will include the design of a 2D fluidized bed, a setup well suited for visual observations, the investigation will be limited to the well known ozone decomposition reaction system.

The scope of the project entails the quantification of the reaction behaviour of FCC catalyst in a 2D bed spanning both the bubbling and turbulent regime. The reaction is catalyzed by Fe_2O_3 impregnated FCC catalyst.

2 Literature survey

This literature survey will be divided into two sections; fluidized bed hydrodynamics and fluidized bed reactor modeling. For brevity the hydrodynamic section will only cover information relating to the bubbling and turbulent regime. An overview of the bubbling regime is given, focusing on the relevant velocities and how the regime acts phenomenologically. This background into the hydrodynamics is vital to fully understand the reactor models. The same type of information about the turbulent regime is conveyed in the proceeding sub-section. The last part of the hydrodynamics literature is a discussion on mass transfer and gas dispersion.

The second section is centred on the reactor models for the bubbling- and turbulent regime as well as a transition model spanning both regimes. The Kunii and Levenspiel model, Grace model, Axially Dispersed Plug Flow model and the Thompson et. al. transitional model will be discussed.

2.1 Hydrodynamics

2.1.1 Bubbling regime

There are 4 distinct regimes that exist for gas-solid fluidization. These are, in order of increasing gas velocity, the Bubbling-, Turbulent-, Fast fluidization- and the Pneumatic transport- Regime. Depending on the Geldart particle classification there is a fifth regime that occurs for Geldart A particles before bubbling fluidization. This regime is referred to as particulate fluidization and it exists between the linear velocities of the minimum fluidization velocity (u_{mf}) and the minimum bubbling velocity (u_{mb}) (Yang, 2003:58). To determine the minimum fluidization velocity the Ergun equations can be used (Levenspiel, 1999:449):

$$150\left(1-\varepsilon_{mf}\right)u_{mf}^{*}+1.75(u_{mf}^{*})^{2}d_{p}^{*}=\varepsilon_{mf}^{3}(d_{p}^{*})^{2} \qquad (2.1)$$

or the Grace (1982) correlation, as quoted by Thompson et. al. (1999):

$$u_{mf} = \frac{\mu}{\rho_g d_p}(\sqrt{27.2^2 + 0.0408Ar} - 27.2) \quad (2.2)$$

The bubbling regime starts at the minimum bubbling velocity (u_{mb}) and ends at the onset of the turbulent regime. For the minimum bubbling velocity the following correlation can be used (Kunii & Levenspiel, 1991:73):

$$u_{mb} = u_{mf}[\frac{2300\rho_g^{0.13}\mu^{0.52}e^{P_{45}}}{d_p^{0.8}(\rho_s - \rho_g)^{0.93}}] \quad (2.3)$$

The bubbling regime is characterized by a distinct lean phase and dense phase. The lean phase manifests itself in the form of bubbles, which form at the distributor and move through the dense phase to the bed surface. For Geldart A particles the bubbles reach a maximum stable size, but for Geldart B particles the bubbles keep on growing until it reaches the bed surface or forms a slug. The velocity, at which a single bubble rises, is given by:

$$u_{br} = 0.711\sqrt{g d_b} \quad (2.4)$$

The overall gas velocity through the lean/bubble phase, u_b, is the result of multiple bubbles rising through the dense phase at any given time. The simplest correlation for u_b is the flow rate balance done by Davidson and Harrison (1963) as quoted by Kunii and Levenspiel (1991:147):

$$u_b = u_o - u_{mf} + u_{br} \quad (2.5)$$

However Kunii and Levenspiel also proposed their own two correlations based on the experimental work done by Werther (1983):

For Geldart A solids with D ≤ 1 m:

$$u_b = 1.55\left[\left(u_o - u_{mf}\right) + 14.1(d_b + 0.005)\right]D^{0.32} + u_{br} \quad (2.6)$$

For Geldart B solids with D ≤ 1 m:

$$u_b = 1.6\left[\left(u_o - u_{mf}\right) + 1.13\left(d_b^{0.5}\right)\right]D^{1.35} + u_{br} \quad (2.7)$$

The greatest volume of gas passes through the bed in the form of bubbles. There are several ways to correlate the volume fraction of the lean phase, also known as the bubble fraction. Kunii and Levenspiel (1991:156-157) gave different equations depending on how fast the bubbles move. Generally the following equation is used for fast bubbles:

$$\psi_L = \frac{u_0 - u_{mf}}{u_b - u_{mf}} \quad (2.8)$$

Thompson et. al (1999) derived Ψ_L by applying a mass balance for their reactor model (discussed in section 2.2.3):

$$\psi_L = \frac{\varepsilon - \varepsilon_{mf}}{1 - \phi_{L,0} - \varepsilon_{mf}} \quad (2.9)$$

With ε, the overall bed voidage, given by Clift and Grace (1985) (Thompson et. al., 1999):

$$\varepsilon = 1 - {(1 - \varepsilon_{mf})}\Big/{\left(1 + \frac{u_0 - u_{mf}}{0.711\sqrt{g d_b}}\right)} \quad (2.10)$$

Their approach takes the trace amounts of solids present in the lean phase, $\Phi_{L,0}$ into account. As the bubbles rise, gas reactant has to diffuse into the catalyst-rich dense phase. In addition to the bubble- and emulsion- phase, researchers like Kunii and Levenspiel proposed the existence of a third phase, a cloud that surrounds the bubble. This cloud separates the lean phase from the dense phase, introducing a second inter-phase mass transfer step.

2.1.2 Turbulent regime

Bi, et. al. (2000) gave a detailed state-of-the-art review for turbulent fluidization. In this article they mention that the existence of the turbulent regime was very controversial. This controversy started when Yerushalmi and Cankurt defined two velocities at which the turbulent regime starts (u_c) and where it is fully developed (u_k). As the velocity through a bubbling bed is increased bubbling becomes more vigorous. This causes the pressure inside the dense phase to fluctuate. The standard deviation of the pressure fluctuations is defined to quantize the intensity of the fluctuations:

$$F_p = \sqrt{\frac{\sum_{i=1}^{N}(P_i-\bar{P})^2}{N}} \Big/ \bar{P} \qquad (2.11)$$

This standard deviation increases up to u_c and then it drops off to a constant value at u_k. (See the illustration in figure 2.1)

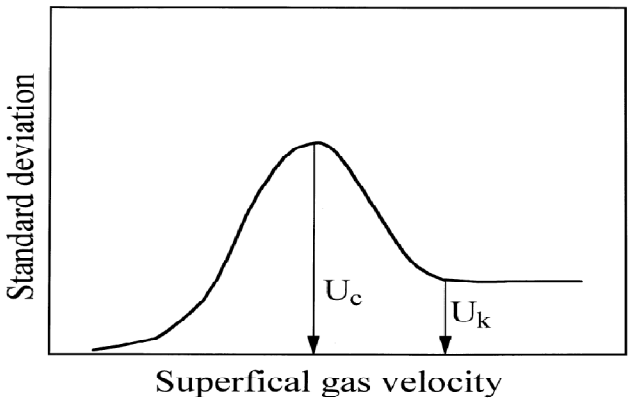

Figure 2.1: Standard deviation of pressure fluctuations used to define u_c and u_k. (Bi et. al., 2000:4792)

The controversy arouse due to the fact that u_k depends on the system used to return entrained particles to the bed. Some researchers found that u_k was at the end of turbulent fluidization and others concluded that u_k does not exist, consequently it is accepted that turbulent fluidization starts at u_c. (Bi et. al., 2000:4793)

Most correlations for u_c have the form of:

$$\frac{d_p \rho_g u_c}{\mu} = m \times Ar^n$$

$$Re_c = m \times Ar^n \qquad (2.12)$$

m is usually smaller than 1 (for u_c correlations) with n usually being close to 0.47 depending on the correlation used. Arnaldos and Casal (1996) gave a full summary of the correlations available in the literature for u_c and u_k. They also state for what particle ranges the respective correlations are valid. Table 2.1 contains some of the correlations. The Bi and Grace (1995) equation in table 2.1 is recommended by Bi et. al. (2000) when absolute pressure fluctuations are used.

2.1.2.1 The end of the turbulent regime

To define the end of turbulent fluidization it is preferable to define the start of fast fluidization. As with the turbulent regime there are two velocities in the literature to define the onset of fast fluidization. The first is the transport velocity (u_{tr}) and the second is the significant entrainment velocity (u_{se}). The transport velocity (u_{tr}) is determined by keeping the linear velocity constant, varying the solids circulation rate and measuring the pressure drop. This procedure is done for several velocities until a graph like figure 2.2 is obtained.

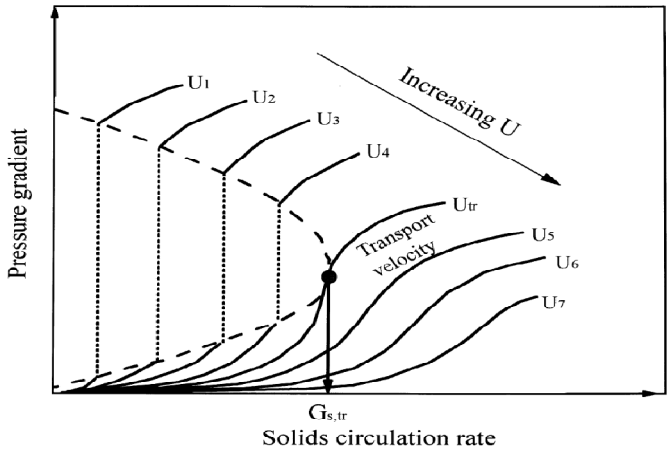

Figure 2.2: Definition of u_{tr} (Bi et. al., 2000:4797).

The determination of u_{se} is less involved and not dependent on the solids circulation rate, but rather the entrainment rate. The linear velocity in the bed is merely increased until the entrainment rate (G_s) starts to increase significantly (see figure 2.3). Table 2.1 lists a few of the correlation summarised by Arnaldos and Casal (1996) which are applicable to this study's particles.

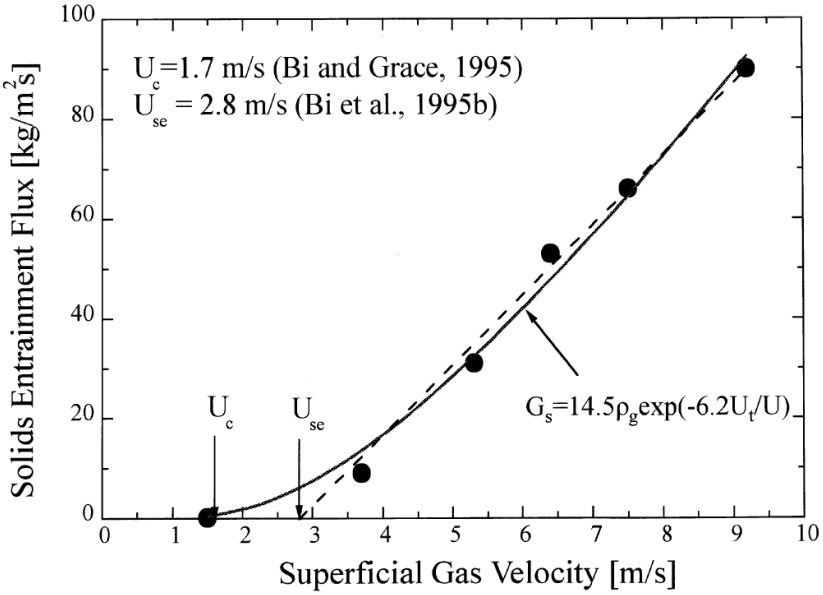

Figure 2.3: Definition of u_{se} (Bi et. al., 2000:4813)

Table 2.1: u_c and u_{tr} correlations (as quoted by Arnaldos and Casal (1996)).

Authors		**Applicable range**
Horio	$Re_c = 0.936Ar^{0.472}$	54<d_p<2600μm
Jin et. al.	$u_c = (gd_p)^{0.5}[\frac{(KD_f)(\rho_s - \rho_g)}{d_p\rho_g}]^{0.27}$ $KD_f = 0.00367$ (for free bed)	50<d_p<1050μm 700<ρ_p<2600kg/m^3
Nakajima et. al.	$Re_c = 0.633Ar^{0.467}$	-
Perales et. al.	$Re_{tr} = 1.41Ar^{0.483}$	A solids
Lee and Kim	$Re_c = 0.7Ar^{0.485}$	0.44<Ar<4.4x10^7 1.22<Ar<5.7x10^7
Bi and Fan	$Re_c = 0.7Ar^{0.485}$	-
Bi and Grace (1995)	$Re_c = 0.565Ar^{0.461}$	-

2.1.2.2 Factors influencing u_c

Firstly the measuring technique can influence u_c. Except for pressure measurements other methods exist for determining u_c. These are the techniques of visual observations, heterogeneity index and bed expansion (Bi et. al., 2000). However, most research groups use pressure fluctuation measurement. Pressure fluctuations can be determined using differential pressure measurement between two points in the dense phase or by using and absolute pressure measurement at one single point in the bed. It is recommended by Bi et. al. (2000) that the absolute pressure measurements are the most consistent measurement and that it agrees well with the visual observations and bed expansion methods. It is also insensitive to axial position where as the differential pressure method is not.

The effect of particle size distribution has been reported by Sun (1991). Figure 2.4 shows the results of this study. A narrower size distribution results in a higher u_c and it is also clear, from figure 2.4, that the static bed height has little effect on u_c. This behaviour was also mentioned by Bi et. al. (2000). It should be noted that the results of figure 2.4 was determined using the differential pressure method at different heights in the reactor and it is clear that u_c is strongly influenced by axial position if this method is used.

Lastly column diameter and bed internals are more factors to be considered. It is reported that u_c decreases with increasing diameter and bed internals lowers the velocity at which u_c normally occurs. (Bi et. al. 2000)

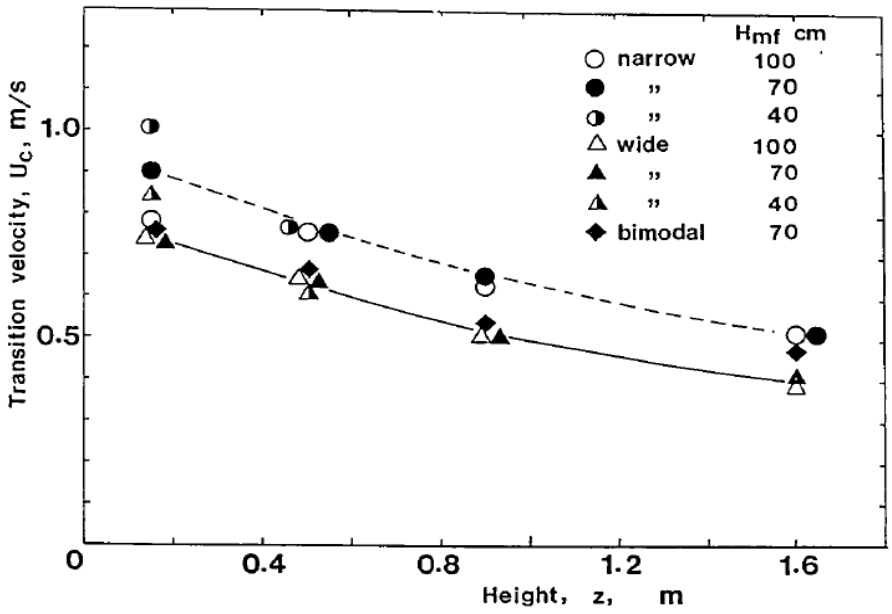

Figure 2.4: The effect of PSD's on u_c. (Sun, 1991)

2.1.3 Mass transfer and gas dispersion

2.1.3.1 Inter-phase mass transfer

Inter-phase mass transfer plays an important role in understanding fluidized beds and in the development of reactor models. The mass transfer coefficient correlations developed by Kunii and Levenspiel for their three-phase model entails two mass transfer steps in series, mass transfer from the bubble phase to the cloud phase (Eq. 2.13) and mass transfer from the cloud to the emulsion phase (Eq 2.14):

$$K_{BC} = 4.5\left(\frac{u_{mf}}{d_b}\right) + 5.85\left(\frac{D_m^{0.5} g^{0.25}}{d_b^{1.25}}\right) \quad (2.13)$$

$$K_{CE} = 6.77\left(\frac{\varepsilon_{mf} D_m u_{br}}{d_b^3}\right) \quad (2.14)$$

These two mass transfer coefficients in series can be combined into one coefficient:

$$\frac{1}{K_{BE}} = \frac{1}{K_{BC}} + \frac{1}{K_{CE}}$$
$$K_{BE} = \frac{K_{BC}K_{CE}}{K_{BC}+K_{CE}} \quad (2.15)$$

Sit and Grace (1981) did mass transfer experiments by using ozone as a tracer and injecting an ozone containing bubble into a 0.56 m wide, 9 mm thick and 2.1 m high 2-D bed. From those experiments a correlation for 3-D beds were derived, which Thompson et. al. (1999) modified by multiplying it with f_{kq}, which seems to be a function of some unknown system parameters:

$$k_q = f_{kq}\left(\frac{u_{mf}}{3} + 2\sqrt{\frac{D_m \varepsilon_{mf} u_b}{\pi d_b}}\right) \quad (2.16)$$

The first term represents convective mass transfer and the second term represents the diffusive mass transfer. For a 2-D bed the convection term of

k_q changes slightly:

$$k_q = f_{kq}\left(0.4\, u_{mf} + 2\sqrt{\frac{D_m \varepsilon_{mf} u_b}{\pi d_b}}\right) \quad (2.17)$$

Foka et. al. (1996) did mass transfer and effective gas dispersion experiments, using irradiated Argon as the tracer to determine the residence time distribution. The experiments were performed from the bubbling to turbulent regime. The authors noted that Grace (1990) suggested using a two phase model to develop correlations for the mass transfer in the turbulent regime. The van Deemter (1961) two phase model was applied to the data and the following correlation, spanning both regimes, was derived:

$$k_g a_I = 1.631 Sc^{0.37} u_0 \quad (2.18)$$

Bi et. al. (2000:4811) mentioned that even though this model is based on a wide range of flow rates, it doesn't account for column geometry and should be used with caution since it has not yet been extensively validated. Chaouki et. al. (1999) used this correlation successfully in a two phase model with an ethylene synthesis reactor operating in the turbulent regime. Other mass transfer correlations suggested by Bi et. al. (2000:4813) are given in Table 2.2 with notes.

Table 2.2: Inter-phase mass-transfer correlation for turbulent beds (Bi et. al., 2000:4813).

Authors	Correlation	Note
Miyauchi et. al. (1980)	$k_g a_I = 3.7 \frac{D_m^{0.5} \psi_L}{d_b^{5/4}}$	Experiments were only conducted in the bubbling regime.
Zhang and Qian (1997)	$k_g = 1.74x10^{-4} Re^{2.14} Sc^{0.81} \frac{D}{d_p}$	Predicts experimental k_g with 14-31% error.

2.1.3.2 Effective gas phase dispersion

In the same article written by Foka et. al. (1996), the gas phase dispersion, from the bubbling to turbulent regime, was determined using a single phase axially dispersed plug flow model. It was concluded that a dispersed plug flow model may not be phenomenologically applicable in a bubbling bed, but it is interesting to note they did discover dispersion follows the same trend as pressure fluctuations, and can also be used to determine u_c (See figure 2.5). Using the data, the authors correlated the Peclet number with:

$$Pe = \frac{7 \times 10^{-2} Ar^{0.32}}{(d_p/D)^{0.4}} \qquad (2.19)$$

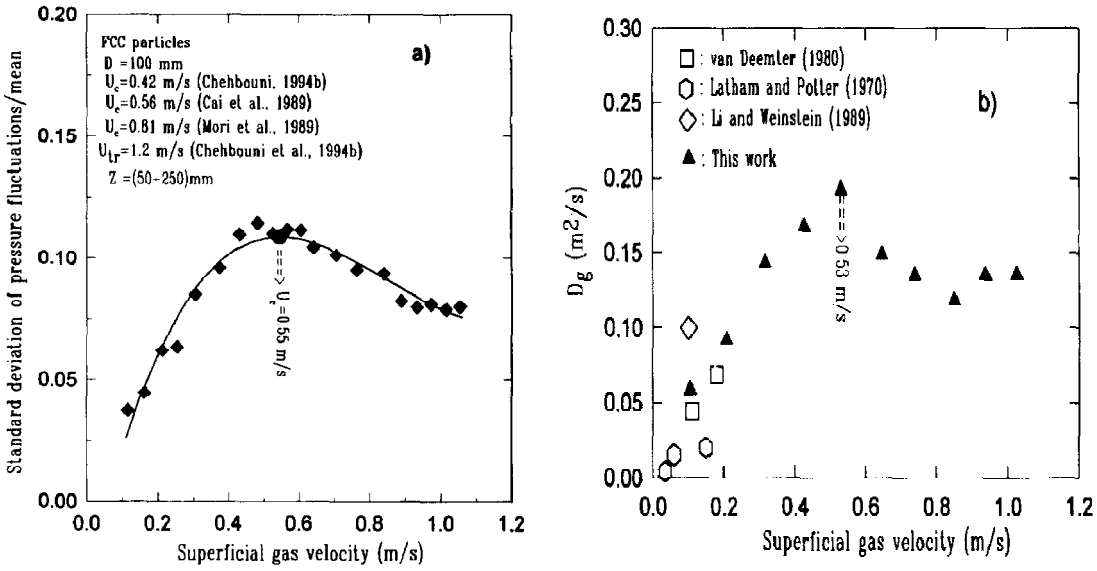

Figure 2.5: (a) Pressure fluctuations versus velocity giving u_c as 0.55 m/s. This compares well with (b), the dispersion coefficient versus velocity which gave u_c as 0.53 m/s. (Foka et. al., 1996)

Other Peclet number correlations, based on single phase axially dispersed plug flow models, which are usually more applicable in the turbulent regime include:

$$Pe = f_{Pe} Ar^{0.32} \left(\frac{D}{d_p}\right)^{0.02344} Sc^{-0.2317} \left(\frac{H_b}{D}\right)^{0.2854} \quad (2.20)$$

(Bi & Grace, 1997 as quoted by Thompson et. al., 1999)

as well as:

$$Pe = 3.47 Ar^{0.149} Re^{0.0234} Sc^{-0.231} \left(\frac{H_b}{D}\right)^{0.285} \quad (2.21)$$

(Bi et. al., 2000)

2.2 Reactor modelling

2.2.1 Bubbling reactor models

There are various reactor models for fluidization depending on the operating regime. For the bubbling regime there are simple two phase models, like the van Deemter (1961) model which assume that the emulsion phase remains at u_{mf} and that no solids are present in the bubble phase. More complex two phase models, like the Kunii and Levenspiel three phase model and the Grace two phase model, does not make these assumption and accounts for reaction in all the phases. The following discussion will be limited to the last two models; as they are widely-accepted in the literature. (Jafari et. al., 2004)

2.2.1.1 The Kunii and Levenspiel Three Phase Model

Kunii and Levenspiel (K-L) developed a three- phase model for reactors operating in the bubbling regime (Levenspiel, 1999:455-460). This model is based on the assumption that a small amount of the gas passes through the dense phase and the rest of the gas bypasses the bed in the form of bubbles. As the bubble moves through the bed reactant diffuses into the dense phase to react on the solid catalyst. The additional phase in the three phase model is a cloud that surrounds the bubble. (Figure 2.6 illustrates the concept of the three phase model.) The mass transfer coefficients based on the bubble volume (K_{BC}, K_{CE}) are also indicated on the illustration. A mass balances over the reactor for the three phase model yields the following equations:

$$C_i = u_b C_{i,B} + u_C C_{i,C} + u_E C_{i,E} \tag{2.22}$$

$$u_b \frac{dC_{i,B}}{dz} = \phi_B R_i(\boldsymbol{C_B}) - K_{BC}\psi_B(C_{i,B} - C_{i,C}) \tag{2.23}$$

$$u_C \frac{dC_{i,C}}{dz} = \phi_C R_i(\boldsymbol{C_C}) + K_{BC}\psi_B\left(C_{i,B} - C_{i,C}\right) - K_{CE}\psi_B(C_{i,C} - C_{i,E}) \tag{2.24}$$

$$u_E \frac{dC_{i,E}}{dz} = \phi_E R_i(\boldsymbol{C_E}) + K_{CE}\psi_B(C_{i,C} - C_{i,E}) \quad (2.25)$$

The reaction rate (R_i) is a function of all the species in the respective phases. An example is power law kinetics using a reaction rate constant based on the volume of solid catalyst:

$$R_i(\boldsymbol{C}) = k_R''' \prod_{j=1}^{N_R} C_j^{n_j} \quad (2.26)$$

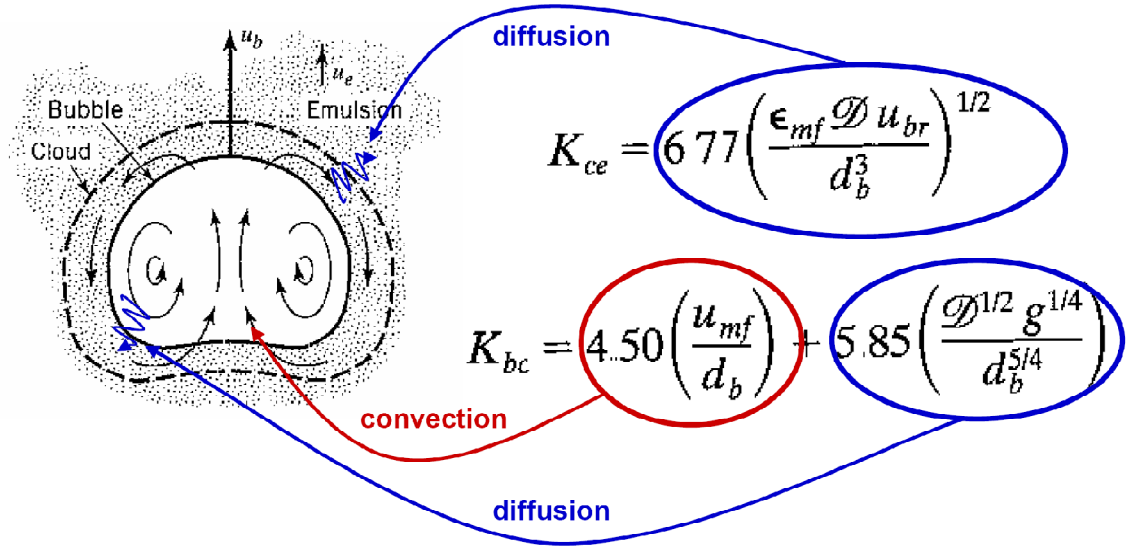

Figure 2.6: Mass transfer for the three phase model (Levenspiel 1999:454).

2.2.1.2 The Grace Two phase model

(Thompson et. al., 1999)

Grace (1984:237-255) proposed a two phase model (G2PB), but with axial dispersion in both phases. Figure 2.7 is a conceptual drawing of a reactor based on this model; variables used are also indicated.

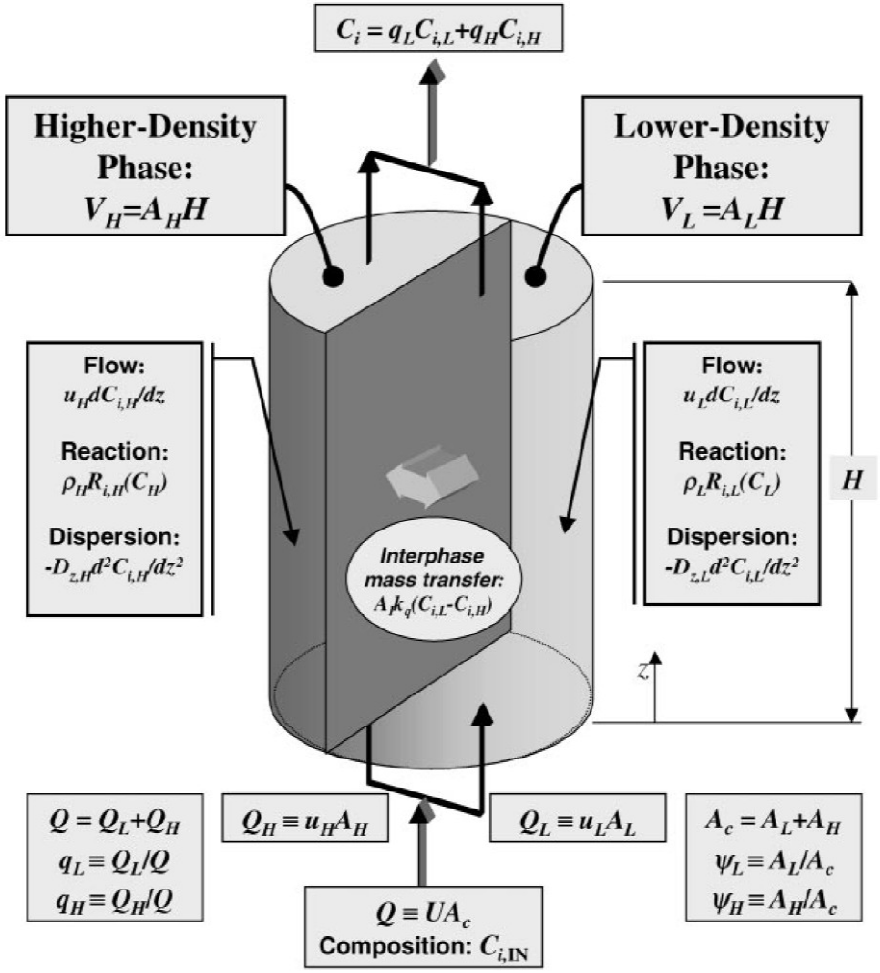

Figure 2.7: Representation of the Grace model. (Thompson et. al., 1999)

A mole balances over the system yields the following equations:

$$C_i = q_L C_{i,L} + q_H C_{i,H} \tag{2.27}$$

$$u_L \frac{dC_{i,L}}{dz} = D_{z,L} \frac{d^2 C_{i,L}}{dz^2} + \phi_L R_{i,L}(\boldsymbol{C_L}) - k_q a_I \varepsilon_L (C_{i,L} - C_{i,H}) \tag{2.28}$$

$$u_H \frac{dC_{i,H}}{dz} = D_{z,H} \frac{d^2 C_{i,H}}{dz^2} + \phi_H R_{i,H}(\boldsymbol{C_H}) + (\frac{\psi_L}{\psi_H}) k_q a_I \varepsilon_L (C_{i,L} - C_{i,H}) \tag{2.29}$$

The boundary conditions at the inlet (z=0) for this model is given by:

$$u_L (C_{i,L,z=0^+} - C_{i,IN}) = D_{z,L} \frac{dC_{i,L}}{dz}_{z=0} \tag{2.30}$$

$$u_H (C_{i,H,z=0^+} - C_{i,IN}) = D_{z,H} \frac{dC_{i,H}}{dz}_{z=0} \tag{2.31}$$

And at the outlet ($z=H_b$):

$$\left.\frac{dC_{i,L}}{dz}\right|_{z=H_b} = 0 \tag{2.32}$$

$$\left.\frac{dC_{i,H}}{dz}\right|_{z=H_b} = 0 \tag{2.33}$$

2.2.2 Turbulent reactor models

Most open literature work on catalytic fluidized bed modelling was performed on the bubbling regime. Turbulent fluidization on the other hand has not received as much attention (Bi et. al., 2000:4814), even though most of the industrial catalytic and non-catalytic reactors operate in this regime (Thompson et. al., 1999). Generally turbulent reactor models are based on one of 4 principles (as quote by Bi et al. 2000:4814):

- A simple CSTR model (Wen, 1984; Hshimoto et. al., 1989).
- A one dimensional ideal PFR model (van Swaaij, 1978; Fane & Wen, 1982).
- A PFR model with axial dispersion (Avidan, 1982; Wen, 1984; Edwards & Avidan, 1986; Li & Wu, 1991; Foka et. al., 1994).
- A Two phase behaviour models (Krambeck et al., 1987; Foka et. al., 1996; Ege, Grislingas & deLasa, 1996; Venderbosch, 1998; Thompson et. al., 1999; Abba et. al., 1999).

Usually two phase models work better if low linear velocities are used and a PFR with axial dispersion is better when working with higher velocities. Two phase models were already discussed, so only the Axially Dispersed Plug Flow Reactor (ADPF) model will be overviewed in this section. A mole balance for this approach simply yields the following:

$$u_0 \frac{dC_i}{dz} = D_{z,} \frac{d^2C_i}{dz^2} + \phi R_i(\boldsymbol{C}) \tag{2.34}$$

With the boundary conditions;

$$u(C_{i,z=0^+} - C_{i,IN}) = D_z \frac{dC_i}{dz}_{z=0} \tag{2.35}$$

$$\frac{dC_i}{dz}_{z=H_b} = 0 \tag{2.36}$$

(Thompson et. al., 1999)

2.2.3 Generalized Bubbling-Turbulent Model

To account for the transition between regimes authors like Thompson et. al., (1999) and Abba et. al. (2003) have suggested generalized/generic models. The Thompson et. al. (1999) generalized bubbling turbulent (GBT) model combine a two phase model for a bubbling bed with an ADPF model for a turbulent bed by using methods of probabilistic averaging. This creates additional complexity, but the models have been proven to work well.

Thompson et. al. (1999) reconciled the Grace Two Phase model with the ADPF model, by using probabilistic averaging to vary parameters continuously as u_o was changed. This was done by differentiating equation 2.27:

$$\frac{dC_i}{dz} = \frac{1}{u}(\psi_L u_L \frac{dC_{i,L}}{dz} + \psi_H u_H \frac{dC_{i,H}}{dz}) \tag{2.37}$$

Note: $q_L = \psi_L.u_L/u_0$ and $q_H = \psi_H.u_H/u_0$

Equation 2.28 and 2.29 is then substituted and the results are manipulated so it can be related to equation 2.34. The following equation shows the result of this manipulation:

$$u\frac{dC_i}{dz} = \alpha_D(z).\left[D_{z,}\frac{d^2C_i}{dz^2}\right] + \alpha_R(z).[\rho R_i(\boldsymbol{C})] \tag{2.38}$$

where:

$$\alpha_D(z) = \left[\psi_L D_{z,L} \frac{d^2 C_{i,L}}{dz^2} + \psi_H D_{z,H} \frac{d^2 C_{i,H}}{dz^2}\right] \Big/ \left[D_z, \frac{d^2 C_i}{dz^2}\right]$$

and:

$$\alpha_R(z) = \left[\psi_L \rho_L R_{i,L}(\boldsymbol{C_L}) + \psi_H \rho_H R_{i,H}(\boldsymbol{C_H})\right] \Big/ \left[\rho R_i(\boldsymbol{C})\right]$$

From this result it is clear that the G2PB model approached the ADPF model when $\alpha_D = \alpha_R = 1$. This will occur in the following limits:

$$\lim_{U \to U_\infty} u_L = \lim_{U \to U_\infty} u_H = u$$
$$\lim_{U \to U_\infty} D_{z,L} = \lim_{U \to U_\infty} D_{z,H} = D_z$$
$$\lim_{U \to U_\infty} \rho_L = \lim_{U \to U_\infty} \rho_H = \rho$$

Therefore three parameters need to vary as u_o is increased, u_L, $D_{z,L}$ and ρ_L. Note that the H-phase parameters u_H, and ρ_H can be calculated from the L-phase parameters using material balances. The H-phase's dispersion, $D_{z,H}$, is assumed to equal the overall D_z calculated from Peclet correlations.

The lean phase bulk density (ρ_L) is related to the solids volume fraction by $\rho_L = \rho_s \Phi_L$, therefore Φ_L can be used instead of ρ_L. To calculate the L-phase parameters a probability density function is used. The probability that the bed is in the turbulent regime is denoted by $P_T(U)$. Thompson et. al. used the limiting cases for when the bed is in the fully bubbling regime and when the bed is in the fully turbulent regime to derive the following equations:

$$u_L = (1 - [P_T(U)])u_b(U) + [P_T(U)].U_0 \quad (2.39)$$
$$D_{z,L} = (1 - [P_T(U)])D_m + [P_T(U)].\frac{U_0 H_b}{Pe(U)} \quad (2.40)$$
$$\phi_L = (1 - [P_T(U)])\phi_{L,0} + [P_T(U)].\phi(U) \quad (2.41)$$

To determine $\Phi_{L,0}$, the L-Phase volume fraction, equation 2.9 was used. The bubble rise velocity correlation of Davidson and Harrison (1962) was modified that $u_b \rightarrow 0$ as $u_0 \rightarrow u_{mf}$:

$$u_b = (u_0 - u_{mf})(1 + \frac{0.711}{u_0}\sqrt{g d_b}) \qquad (2.42)$$

The Peclet number used was that of Bi and Grace (1997) (equation 2.20). $P_T(U)$ was determined using an u_c correlation and the standard deviation of the data on which the correlation was based. Thompson et. al. (1999) applied this model to predict the experimental results of Sun (1991). The model succeeded in predicting the results with very good accuracy.

3 Experimental setup

3.1 Equipment

A two dimensional column with a thickness of 25 mm, width of 0.4 m and a height of 4.5 m was used for the experiments. A primary and secondary cyclone was used to increase the solids return efficiency. The primary cyclone is a volute cyclone, due to high solids loading while the secondary cyclone is a tangential cyclone. Appendix A contains the engineering drawings of the column. A triangular pitch perforated plate distributor with 35 2 mm holes was used. A porous cloth was placed below the distributor to prevent solids weepage. This increased the pressure drop which improved the gas distribution over the distributor. For all velocities the pressure drop over the distributor was greater than the pressure drop over the bed.

Figure 3.1 shows the overall experimental setup. Vortex flow meters were installed, however due to the volumetric flow range of the meters; two meters were installed. The smaller flow meter was used for the linear velocity range of 0.1 m/s to 0.6 m/s. The larger one of the two has a range of 0.6 m/s to 2.0 m/s, although the upper part of this range was not used for this study. For velocities lower than 0.1 m/s a rotameter was employed.

Differential Pressure meters were installed over the distributor and the cyclones. It is noteworthy that the volute cyclone had a pressure drop 10 times less than what was predicted using cyclone pressure drop correlations. This caused problems with the overall pressure balance of the setup, which was corrected by installing a flow restriction in the dipleg of the secondary cyclone. Filter bags were placed after the secondary cyclone to capture unseparated solids. The cyclones achieved a good efficiency and the initial loss of solids was less than 4%, since these solids where capture within the first two hours of operation it was concluded that the solids were fines and nearly no solids were lost during the experiments. A Pressure transmitter was installed at a height of 0.3 m, which was below the bed surface.

The fluidizing medium was air supplied by a compressor. The compressor has a chiller maintaining the air at a constant temperature of 15 ˚C. The air was dosed with ozone that was generated using the EcoTec MZV1000 cold corona ozone generator. Pure oxygen was used instead of air to decrease the likelihood of NO_x gasses forming. The inlet concentration was determined by taking a sample from the plenum chamber. The sampling probe was inserted to draw a sample from the centre of the plenum chamber and glass beads were added to the plenum chamber to ensure good gas mixing and distribution. The linear velocity in the column was not affected by the sampling flow rate, as the volumetric sampling flow rate was small relative to the overall volumetric flow rate (measured before the plenum chamber and from which the linear velocity is calculated). The outlet sample was drawn 4.1 m above the distributor, also from the centre of the column. The samples were continuously analysed using the 2B Technologies Inc. UV-106 ozone analyser. Ozone analysis is done by the well established method of light absorption at a wavelength of 254 nm.

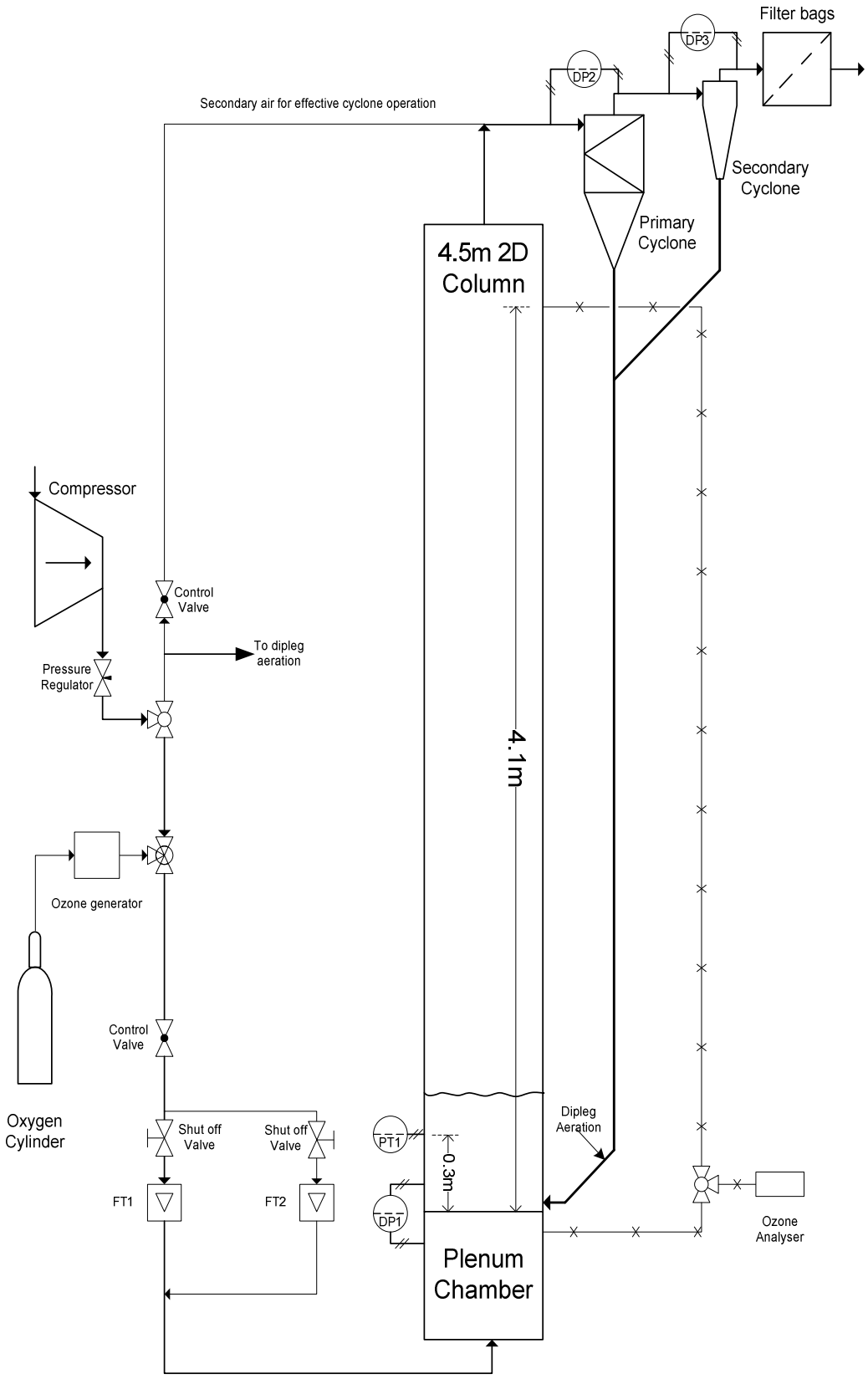

Figure 3.1: The piping and instrumentation setup.

3.2 Ozone decomposition reaction

Ozone is thermodynamically favoured to decompose to oxygen. The heat of reaction is ΔH_{298} = -138 kJ/mol and free energy of reaction is ΔG_{298} = -163 kJ/mol. Ozone is thermally stable up to 523K; therefore its decomposition at low temperature needs to be catalyzed. Generally, metals and metal oxides can serve as a catalyst. The metal oxides are more active than the metals on a mass basis. The order of activity for the different metal oxides is as follow:

$$Ag_20 > NiO > Fe_2O_3 > Co_3O_4 > CeO_2 > Mn_2O_3 > CuO > Pb_2O_3 > Bi_2O_3 > SnO_2 > MoO_3 > V_2O_5 > SiO_2$$

(Dhandapani and Oyama, 1997:137)

At O_2 concentration of less than 50% and water vapour less than 4%, the reaction rate displays zero order kinetics towards O_2 and H_2O (Dhandapani and Oyama, 1997:138). The reaction rate constant for several studies are shown in table 3.1, all of which found first order kinetics sufficient to fit the data. Important to note, is each of these results was obtained with catalyst the authors prepared themselves, explaining the large variations.

Table 3.1: Rate constants for the decomposition of ozone.

Article	Value	Units
Fan et al (2008)	98 x 10^{-6}	m^3gas/(kg(cat).s)
Schoenfelder et al (1996)	1000x10^{-6} to 3000x10^{-6}	m^3gas/(kg(cat).s)
Pagliolico et al (1992)	44.7	m^3gas/(m^3(cat).s)
Sun & Grace (1990)	1 to 9	m^3gas/(m^3(cat).s)
Fryer & Potter (1976)	0.05 to 7.75	m^3gas/(m^3(cat).s)

3.2.1 Catalyst Preparation

Most studies impregnated Ferric Oxide onto a support particle; the support can be anything from FCC catalyst to sand. The preparation method entails

adding the support particles to a mixture of 10 %(wt) Ferric Nitrate solution and stirring for 1 hour. It is then calcinated at 450 ˚C for approximately 1.4 hours, until all the NO_2 gasses are released. (Sun & Grace, 1990) Equation 2.41 shows the reaction that takes place to deposit Fe_2O_3 on the catalyst support. (Fan et. al., 2008)

$$Fe(NO_3)_3.nH_2O \xrightarrow{\geq 370℃} \frac{1}{2}Fe_2O_3 + 3NO_2 + \frac{3}{4}O_2 + nH_2O \qquad (2.41)$$

Repeating this method on the specific FCC catalyst sample employed in this study resulted in a low catalyst activity of 0.71 s^{-1}. Different modifications where made to see if the activity could be increased and will be discussed in the results section.

To determine the catalyst activity a small packed bed reactor was used. The reactor was 50 mm in height with an internal diameter of 16.4 mm. Approximately 6 g of catalyst was added to the reactor. Peclet calculations suggested the flow rate should be above 15 ml/s to ensure plug flow behaviour. The ozone analyser had a response time of 5 seconds. The time required to ensure that steady state is reached and an average reading of steady state can be taken was 10 minutes. Therefore the inlet concentration and outlet concentration was measured for 10 min respectively. The weight of catalyst and the volumetric flow rate was varied to confirm the first order assumption.

3.3 Method

For the experimental runs 5 kg of catalyst was loaded into the column. About 0.2 kg of fines was initially caught in the filter bags over a period of 2 hours. It was also determined that 0.75 kg of catalyst was in the return system (Approximately 15%). The height of the bed before fluidization was 0.53 m. Samples of the catalyst were taken at the beginning of the experiment, after 3 hours, 5 hours, 10 hours and 12 hours, to test for catalyst deactivation.

After start-up, the ozone measurement took 30 - 45 minutes to reach steady state, inlet ozone concentrations where in the range of 20 – 80 ppm. Flow rate was then adjusted to the desired linear velocity and the inlet concentration of ozone was measured for 15 min and then switched to the outlet probe for 15 minutes. All the instrumentation had a 4-20 mA signal output that was logged on a computer using a National Instruments USB-6008 analogue signal data logger. Readings were recorded at a rate of 1 kHz; the pressure transmitter was specifically selected to have a response time of 1 kHz. These pressure transmitter readings were used to determine u_c by the method described in section 2.1.2.

4 Results

4.1 Determination of u_c

The onset of turbulent fluidization (u_c) was determined using the method of absolute pressure fluctuations. The pressure transmitter was located 0.3 m above the distributor. Runs were performed before and during the reaction experiments. A total of 6 runs were done and the result is reported in figure 4.1 as u_c = 0.4 m/s.

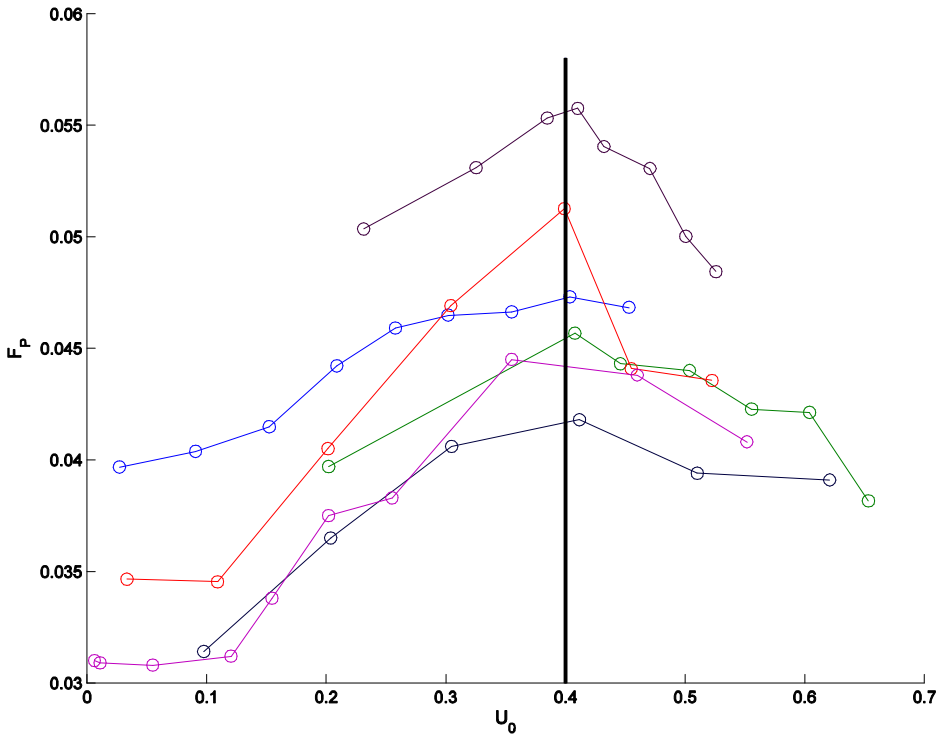

Figure 4.1: Datasets of 6 runs for determining u_c.

Correlations predicted an u_c in the range of 0.5 m/s to 0.65 m/s. The difference is most likely due to the wall effects and the specific catalyst properties. It is known that smaller diameter reactors and bed internals decrease u_c (see section 2.1.2.2) and the limited third dimension in this study might result in a similar behaviour, where the solids are forced to move

more violently into the unrestricted directions; hence turbulent fluidization is achieved faster.

4.2 Catalyst preparation

4.2.1 Required activity

In order to maximise the effect of inter-phase mass transfer, the catalytic activity can be manipulated for the specific weight of catalyst employed in the column. The best way to quantify the effects of mass transfer on reactor performance is to compare it with the maximum achievable conversion (PFR for a first order reaction). Therefore the conversion is divided by the conversion that can be achieved in an ideal PFR with the same amount of catalyst. Very low catalyst activities will imply negligible mass transfer effects, while too high activities will result in the PRF and true conversion being to close to unity thereby reducing resolution on the "x_{real}/x_{PFR}" - axis. The graph in figure 4.2 depicts the reaction behaviour on as a function of catalyst activity. The model of Thompson et. al. is used, with the 2D column mass transfer coefficient of Sit and Grace (equation 2.17 with $f_{kq} = 1$), the Bi and Grace correlation for the Peclet number (equation 2.20 with $f_{Pe} = 1$) and with $u_c = 0.4$ m/s. The mass of catalyst was 5 kg, with 15 % of the catalyst in the return system.

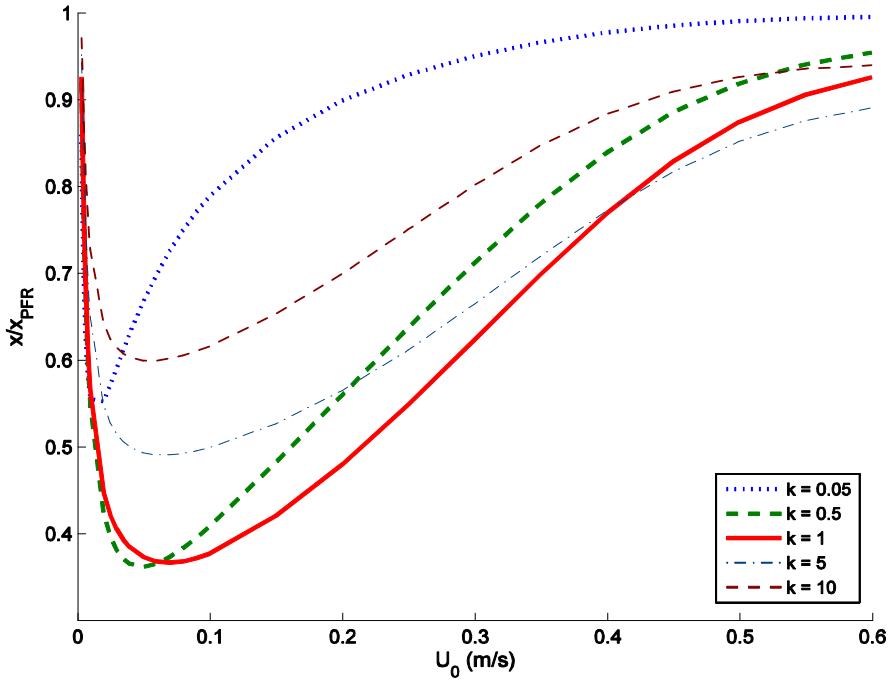

Figure 4.2: Simulated results using the Thompson et. al. model to illustrate the effect of different catalyst activities.

From this graph it is evident that two effects need to be considered: the width and depth of the parabolic dip. The dip can be attributed to the two phase mass transfer of the bubbling regime. It can be observed that as the catalyst activity decreases the width of the parabola decreases. This means that a slight velocity change will cause a major change in the y-axis value, thus returning quickly towards ideal PFR behaviour. The depth effect is related to the range of the x/x_{PFR} values. The turning point of the parabola decreases up to a point as the catalyst activity is decreased and then increases again. It was concluded that a catalyst activity between 0.5 s^{-1} and 1 s^{-1} will be optimal, since major x/x_{PFR} deviations occurs over an extended velocity range.

4.2.2 Obtaining the desired activity

As previously mentioned the method used by Sun and Grace (1990) in conjunction with the FCC catalyst of this investigation resulted in the first

order rate constant, k_r, being 0.71 s^{-1} at 15 ˚C, which was significantly lower than the reported value by Sun and Grace (1990) of 9 s^{-1}. A more active catalyst will be more advantageous since dilution with inert solids can be used to manipulate the activity accordingly. Different modifications to the impregnations procedure were made and the results are shown in table 4.1. Wet catalyst had a clay-like consistency and baked to solid chunks in the furnace. This problem was solved by first drying the catalyst overnight before placing it in the furnace. No change in the activity was observed (run 6 versus run 7). Figure 4.3 shows the first order fit to the data for run 6. The data on runs 1 to 5 can be found in appendix B.

Table 4.1: Summary of catalyst impregnation trails to increase catalyst activity.

Run	[Ferric Nitrate]	Soaking Time	Calcination Temp.	Calcination Time	k_r
1	10 %(wt)	1h	450 ˚C	1.4 h	0.71 s^{-1}
2	5 %(wt)	1h	450 ˚C	1.4 h	0.71 s^{-1}
3	5 %(wt)	12h	450 ˚C	1.4 h	0.80 s^{-1}
4	5 %(wt)	1h	500 ˚C	1.4 h	0.70 s^{-1}
5	5 %(wt)	1h	475 ˚C	2 h	0.96 s^{-1}
6	5 %(wt)	Stir 2h	475 ˚C	2 h	1.09 s^{-1}
7	5 %(wt)	Stir 2h and Dry 12h	475 ˚C	2 h	1.10 s^{-1}

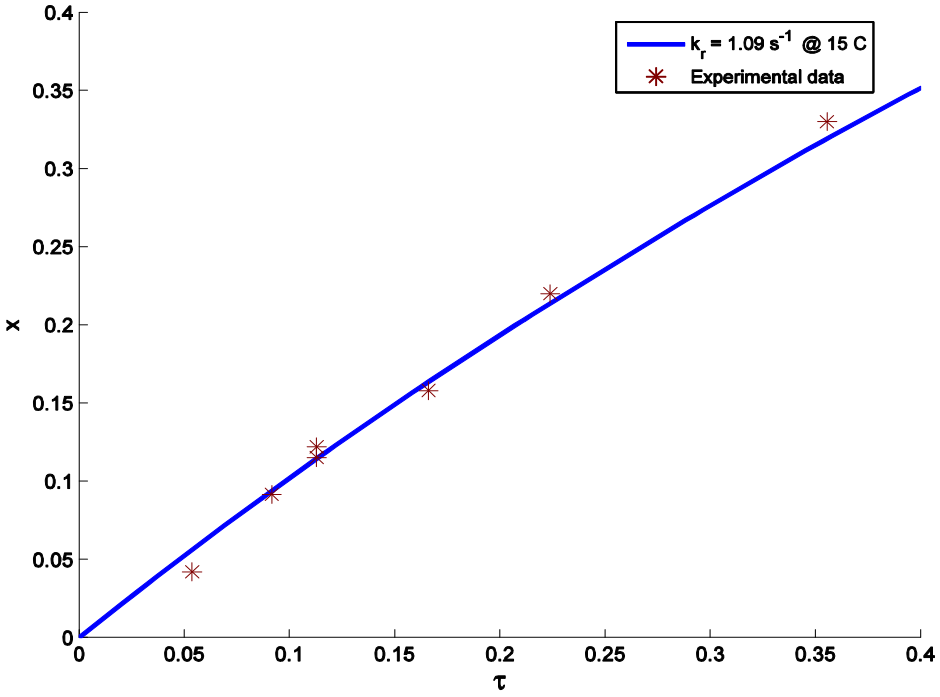

Figure 4.3: First order fit to experimental data with k_r = 1.09 s^{-1}, at 15 ˚C (R^2 = 0.9932).

4.3 Catalyst deactivation

From the literature it is well established that ozone decomposition catalyst deactivates. Two types of deactivation trends where noted. Sun (1991:40), who used FCC impregnated with Fe_2O_3 observed a constant deactivation of 3% per hour. Heisig et. al. (1997) had the same type of deactivation. The second deactivation trend is where the catalyst activity reaches a plateau. The results of an investigation done by Dhandapani and Oyama (1997) showed the catalyst had an initial deactivation but reached a point where the activity of the catalyst remained constant.

The activity of the catalyst samples taken from the reactor were analysed and it was found that the catalyst followed the plateau trend, as show in figure 4.4. The catalyst had a stable operating life-time of about 12 hours.

Only the data generated during the constant activity plateau is reported in this study.

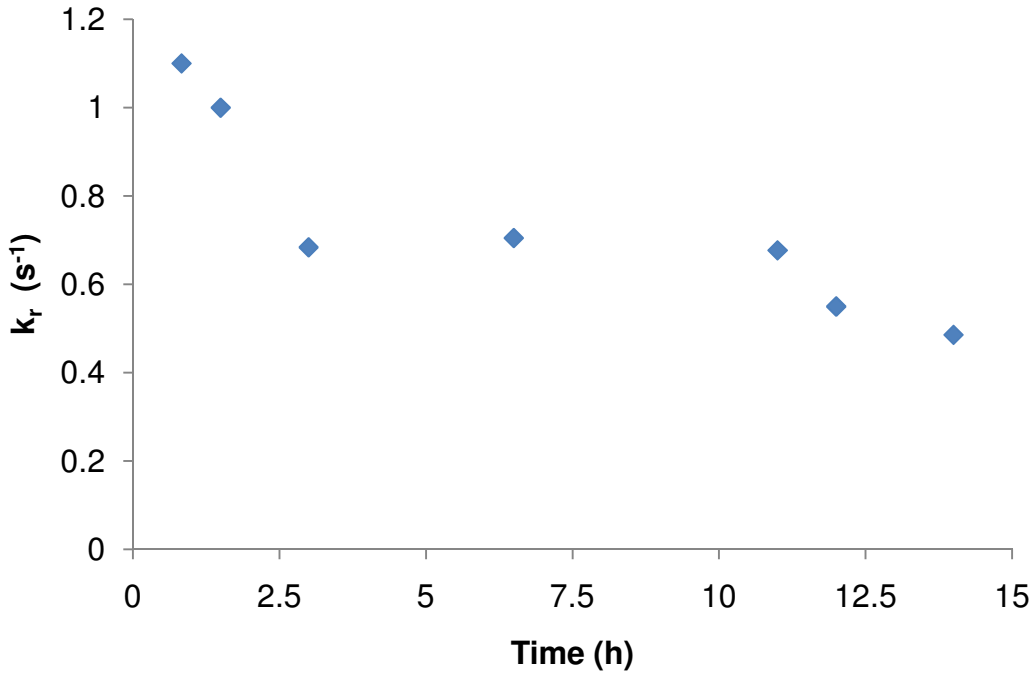

Figure 4.4: Deactivation profile of the first order rate constant.

4.4 2D FBR experimental results

4.4.1 Reactor performance

Due to the limited lifetime of the catalyst two sets of useful data was obtained. Figure 4.5 shows the results of the data. Note that ozone readings fluctuated during the sampling time (10 minutes) and are indicated on the figure.

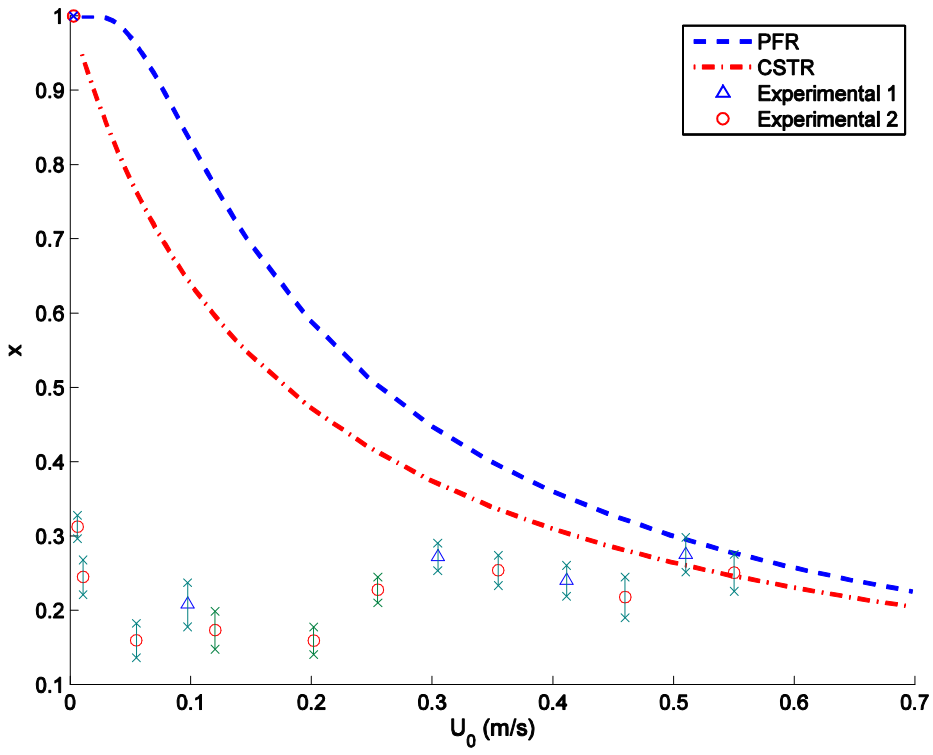

Figure 4.5: Conversion data with the standard deviation of the measured fluctuation.

It is clear from the first two data points that upon entry into the bubbling regime there is a major drop in the conversion due to the inter-phase mass transfer effect. The data can be better visualised by employing the method discussed in section 4.2.1, where the conversion is plotted as a fraction of the optimum conversion on the y-axis (see figure 4.6).

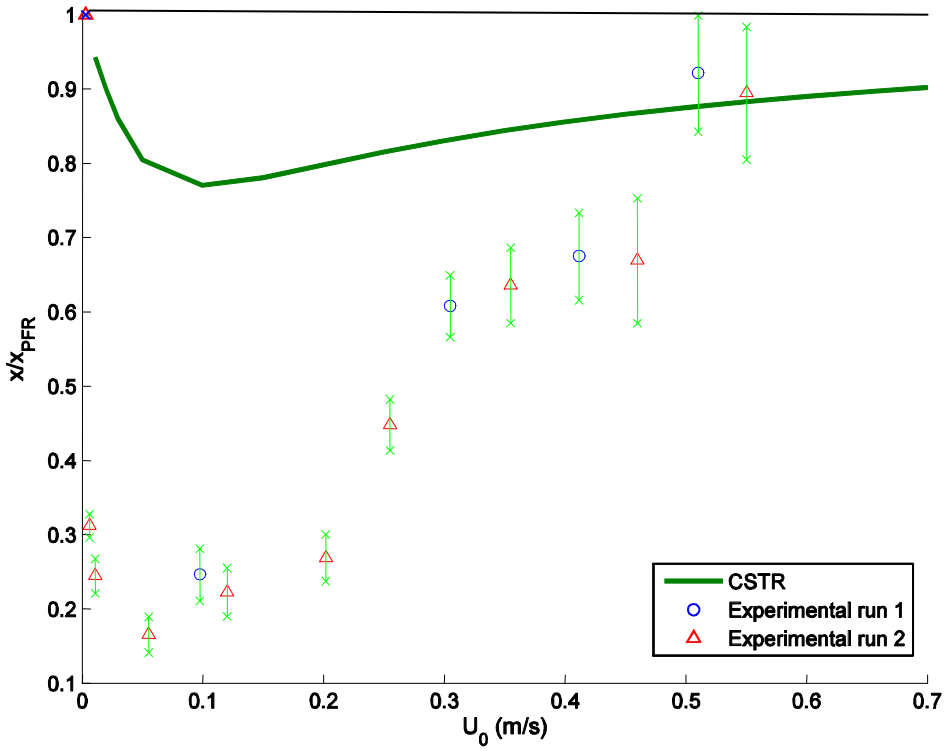

Figure 4.6: The x/x_{PFR} plot of the experimental data.

In figure 4.7 the Thompson et. al. model is compared to the data. The bubble size used was 8.5 cm, u_c was 0.4 m/s and the Sit and Grace 2D mass transfer correlation was used. It is evident that the mass transfer effect in the bubbling regime is under predicted. To fit the Sun (1991) data Thompson et. al. employed a correction factor for the mass transfer coefficient (f_{kq}) and the Peclet number (f_{Pe}). Manipulation of these two variables resulted in a good fit, both in the case of the Thompson et. al. investigation and in this investigation. But it should be noted that the correction factors used to fit the experimental data did not correspond to those used by Thompson et. al. The crucial fitting parameter f_{kq} used for scaling the mass transfer coefficient was found to be less than that of the original correlation (f_{kq} = 0.25), while Thompson fitted a parameter twice the size of the original correlation (f_{kq} = 2.023). An f_{Pe} of 1 was deemed sufficient; it had a negligible effect on the model.

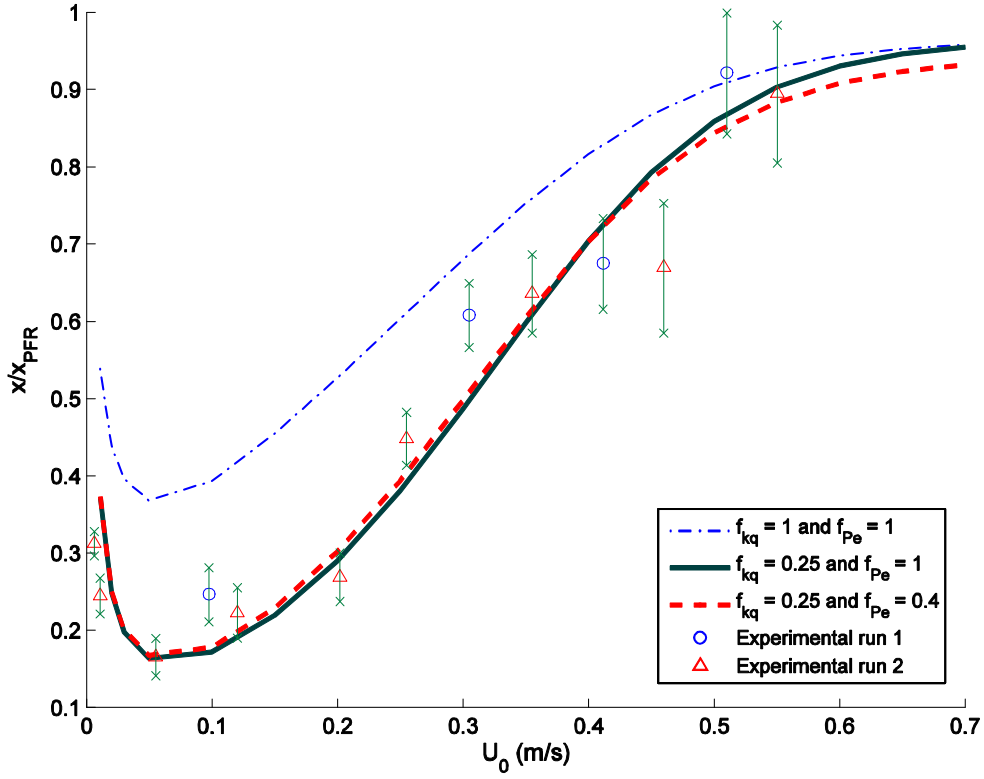

Figure 4.7: The Thompson et. al model with different correction factors.

The Thompson et. al model was used in conjunction with different mass transfer correlations discussed in section 2.1.3.1 and the result can be seen in figure 4.8. It is evident that all three correlations resulted in reasonable fits without any parameter adjustments. None of these correlations are geometry specific, so the same correlation is used for 2D and 3D columns.

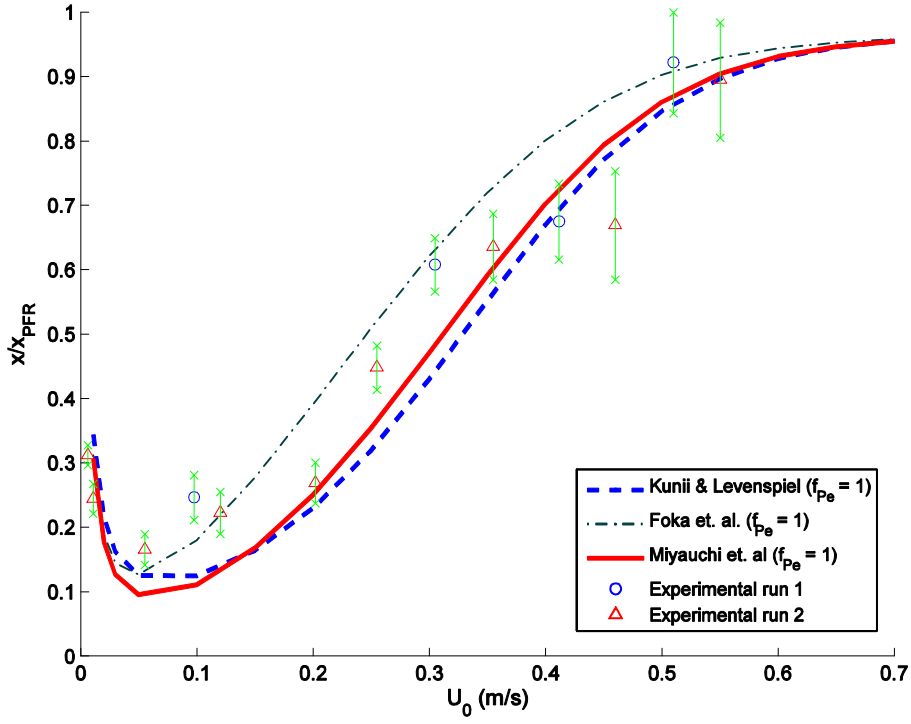

Figure 4.8: Good model-data agreement, without parameter adjustment, using the Kunii and Levenspiel (Eq. 2.15), Foka et. al. (Eq. 2.18) and Miyauchi et. al. (first equation of table 2.1) mass transfer correlations in combination with the Thompson et. al. model.

An interesting observation from the data is the sudden increase in conversion at velocities exceeding 0.45 m/s. This might be attributed to experimental error and the limited data of this study is not sufficient to confirm the discontinuity. This said; there might be significance in the observation, hinting that sudden mass transfer enhancement or TDH reaction contribution is achieved at a specific velocity. If the phenomenon exists it would not have manifested in the reaction work by Sun (1991) due to the high catalyst activities in that study. Figure 4.9 shows the “pinching” of the conversion data. More experimental work is required to substantiate the suspicions.

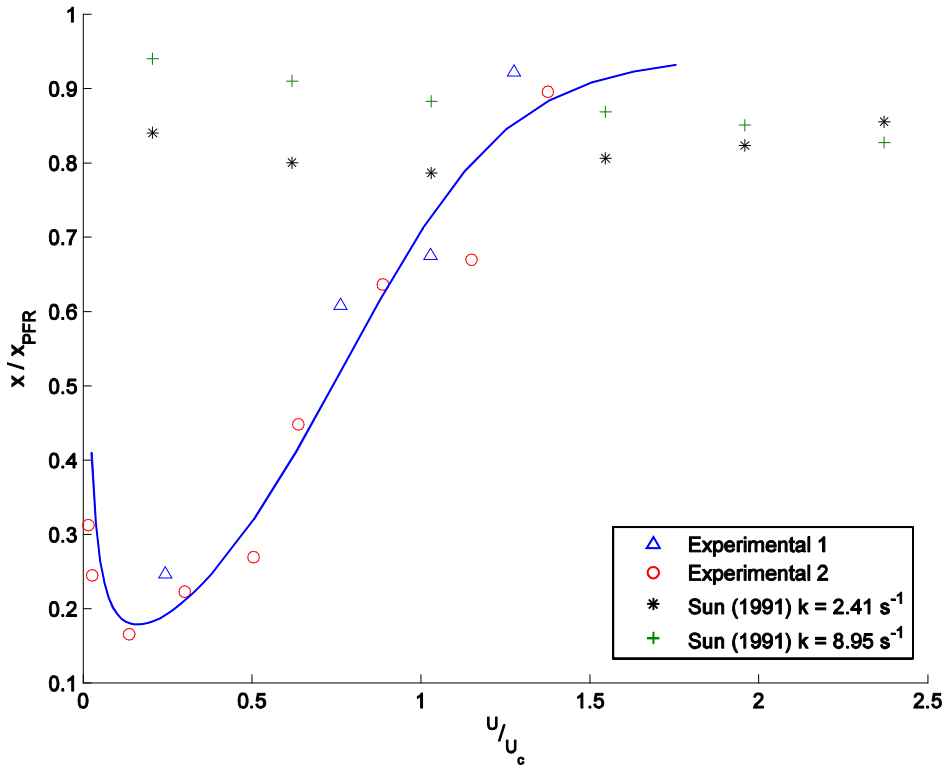

Figure 4.9: A comparison of this study's data with the Sun (1991) data.

5 Conclusions and Recommendations

5.1 Conclusions

The ozone reaction was used to study the reactor performance of a 25cmx40cmx450cm two dimensional fluidized bed reactor operating in the bubbling to turbulent regime. This was used as an indirect method to evaluate the mass transfer and dispersion characteristics in the reactor. The following conclusions can be made:

- The effect of inter-phase mass transfer on reaction performance was clearly observed in the experimental data.
- The design of the reactor system, catalyst activity and catalyst life-time allowed for decent quantification of reaction performance differences.
- The turbulent onset velocity, u_c, was lower (0.4 m/s) than correlations predicted, as well as what previous researchers found (Sun (1991) found it to be 0.485 m/s). This might be due to the wall effects of the 2D column.
- The Thompson et. al. model in conjunction with the Sit and Grace (1981) correlation under predicted the inter-phase mass transfer, but gave a very good fit to the data using a scaling factor. The Kunii and Levenspiel (1991), Foka et. al. (1996) and Miyauchi et. al. (1980) mass transfer correlations in combination with the Thompson et. al. model showed good agreement with the data, without the need for prior knowledge of the conversion.
- The gradual improvement of reactor performance with an increase in superficial velocity, as predicted by the Thompson et. al. model, was not observed. Instead a discontinuity in the vicinity of u_c was noted.

5.2 Recommendations

From this study the following recommendations are made for future studies:

- It is recommended that a future study be done on the same system, focusing on the transitional area between the bubbling and turbulent regime. The discontinuity in the vicinity of u_c should be investigated by separating the TDH's reaction contribution from that of the bed.
- The study should be extended to a 3D column in order to clarify the geometry effects on reaction performance and u_c.

6 References

Abba, IA, Grace, JR and Bi, HT (2003) "Spanning the Flow Regimes: Generic Fluidization-bed Reactor Model" *AIChE Journal*, 49(7), 1838-1848.

Arnaldos, J and Casal, J (1996) "Prediction of Transition Velocities and Hydrodynamical Regimes in Fluidization Beds" *Powder Technology*, 86, 285-298.

Bi, HT, Ellis, N, Abba, IA and Grace, JR (2000) "A State-of-the-art Review of Gas-Solid Turbulent Fluidization" *Chemical Engineering Science*, 55, 4789-4825.

Chaouki, J, Gonzalez, A, Guy, C and Klvana, D (1999) "Two-phase Model for a Catalytic Turbulent Fluidized-bed Reactor: Application to Ethylene Synthesis" *Chemical Engineering Science*, 54, 2039-2045.

Dhandapani, B and Oyama, ST (1997) "Gas Phase Ozone Decomposition Catalyst" *Applied Catalysis B: Enviromental*, 11, 129-166.

Fan, C, Zhang, Y, Bi, X, Song, W, Lin, W and Luo, L (2008) "Evaluation of Downer Reactor Performance by Catalytic Ozone Decomposition" *Chemical Engineering Journal*, 140, 539-554.

Foka, M, Chaouki, J, Guy, C and Klvana, D (1996) "Gas Phase Hydrodynamics of a Gas-Solid Turbulent Fluidized Bed Reactor" *Chemical Engineering Science*, 51(5), 713-723.

Fryer, C and Potter, OE (1976) "Experimental Investigation of Models for Fluidized Bed Catalytic Reactors" *AIChE Journal*, 22(1), 38-47.

Grace, JR (1984) "Generalized Models for Isothermal Fluidized Bed Reactors" in Doraiswamy, LR (Editor), *Recent advances in the Engineering Analysis of Chemically Reacting Systems*, New Delhi: Wiley Eastern.

Grace, JR (1990) "High Velocity Fluidized Bed Reactors" *Chemical Engineering Science,* 45(8), 1953.

Heidel, K, Schugerl, K, Fetting, F and Schiemann, G (1965) "Einfluβ von mischungsvorgängen auf den umsatx bei der äthylenbydrierung in flieβbetten" *Chem Engng Sci,* 20, 557-585

Heisig, C, Zhang, W and Oyama, ST (1997) "Decomposition of ozone using carbon-supported metal oxide catalyst" *Applied Catalysis B: Environmental*, 14, 117-129.

Jafari, R, Sotudeh-Gharebagh, R, and Mostoufi, N (2004) "Performance of the Wide-ranging Models for Fluidized Bed Reactors" *Advanced Powder Technology*, 15(5), 533-548.

Kunii, D and Levenspiel, O (1991) *Fluidization Engineering* 2nd Edition, Boston: Butterworth-Heinemann, London: Marine Technology Directorate.

Levenspiel, O (1999) *Chemical Reaction Engineering*, 3rd Edition, New York: Wiley.

Massimilla, L and Johnstone, HF (1961) "Reaction kinetics in fluidized beds", *Chemical Engineering Science*, 20, 105-115.

Miyauchi, T, Furusaki, S, Yamada, K and Matsumura, M (1980) "Experimental determination of the vertical distribution of contact efficiency inside fluidized catalysts" in JR Grace and JM Matsen, *Fluidization* (571-585), New York: Plenum Press.

Ouyang, S, Lin, J and Potter, OE (1993) “Ozone decomposition in a 0.254 m diameter circulating fluidized bed reactor” *Powder Technology,* 74, 73-78.

Pagliolico, S, Tiprigan, M, Rovero, G and Gianetto, A (1992) “Pseudo-Homogeneous Approach to CFB Reactor Design” *Chemical Engineering Science*, 47(9-11), 2269-2274.

Saxena, SC and Jadav, S (1983) “A Two-Dimensional Gas Fluidized Bed for Hydrodynamic and Elutriation Studies” *Powder Technology*, 36, 61-70.

Schoenfelder, H, Kruse, M and Werther, J (1996) “Two-Dimensional Model for Circulating Fluidized-Bed Reactors” *AIChE Journal*, 42(7), 1875-1888.

Shen, CY and Johnstone, HF (1995) “Gas Solid Contacting in Fluidized Beds” *AIChE Journal*, 1, 349-358.

Sit, SP and Grace, JR (1981) “Effect of bubble interaction on interphase mass transfer in gas fluidized beds” *Chemical Engineering Science*, 36, 327-335.

Sun, G (1991) *Influence of Particle Size Distribution on the Performance of Fluidized Bed Reactors* Ph.D thesis, University of British Columbia, Vancouver.

Sun, G and Grace, JR (1990) “The Effect of Particle Size Distribution on the Performance of a Catalytic Fluidized Bed Reactor” *Chemical Engineering Science*, 45(8), 2187-2194.

Thompson, ML, Bi, H and Grace, JR (1999) “A Generalized Bubbling/Turbulent Fluidized-Bed Reactor Model” *Chemical Engineering Science*, 54, 2175-2185.

Van Deemter, JJ (1961) “Mixing and contacting in gas-solid fluidized beds” *Chemical Engineering Science,* 13, 143-154.

Yang, W-C (Editor) (2003) *Handbook of Fluidization and Fluid-Particle Systems* New York: Marcel Dekker.

Zhang, X and Qian, Y (1997) “Mass-transfer Between the Bubble and Emulsion Phase in a Turbulent Fluidized Bed with FCC Particles” in Q Yu and C Huanqin, *Advances in Environmental Engineering and Chemical Engineering* (190-193), Guangzhou, China: South China University of Technology Press.

7 Appendixes

Appendix A: Engineering drawings for a 2D fluidized bed

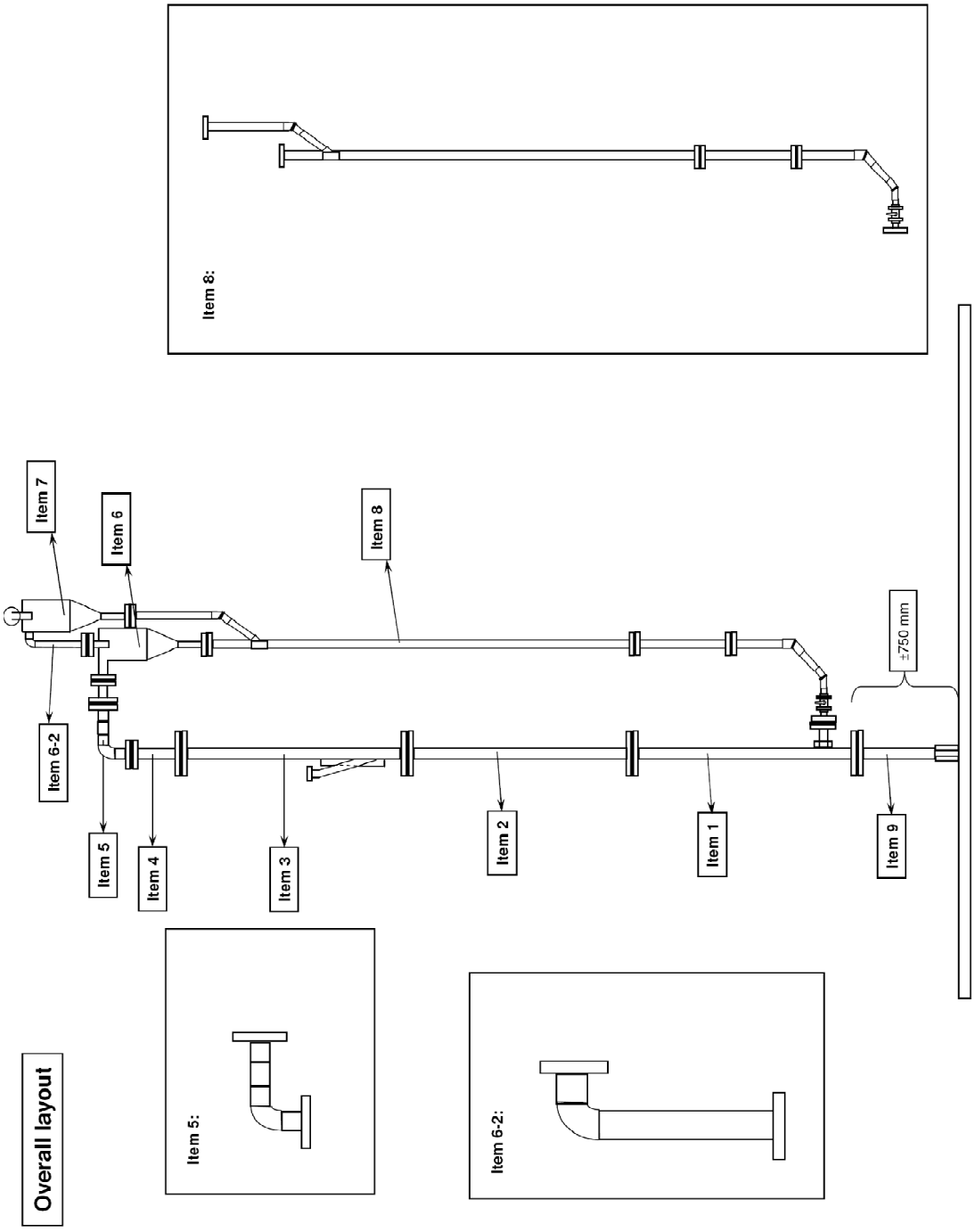
Item 8:
Item 7
Item 6
Item 8
±750 mm
Item 6-2
Item 5
Item 4
Item 3
Item 2
Item 1
Item 9
Item 5:
Item 6-2:
Overall layout

Details for item 1

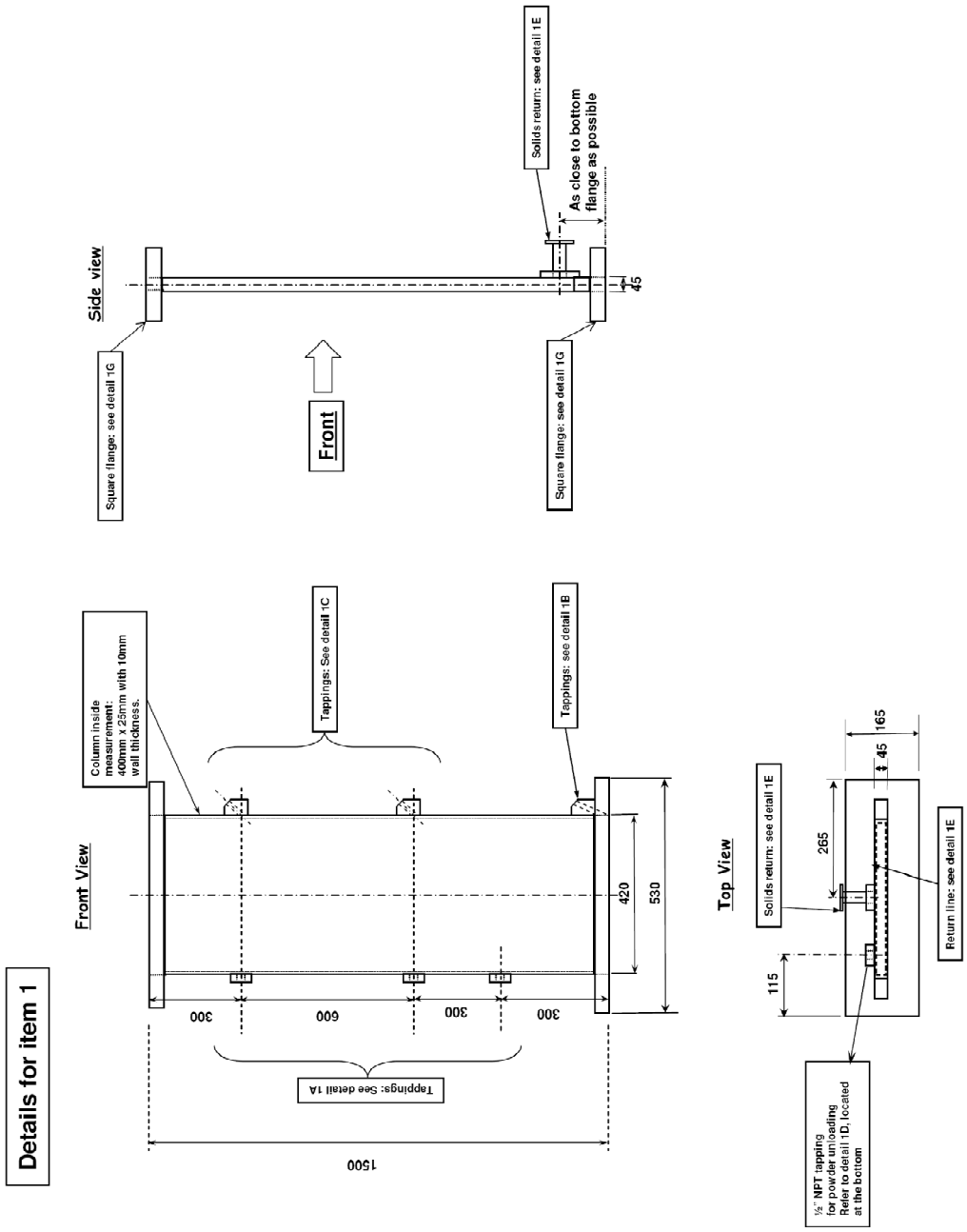

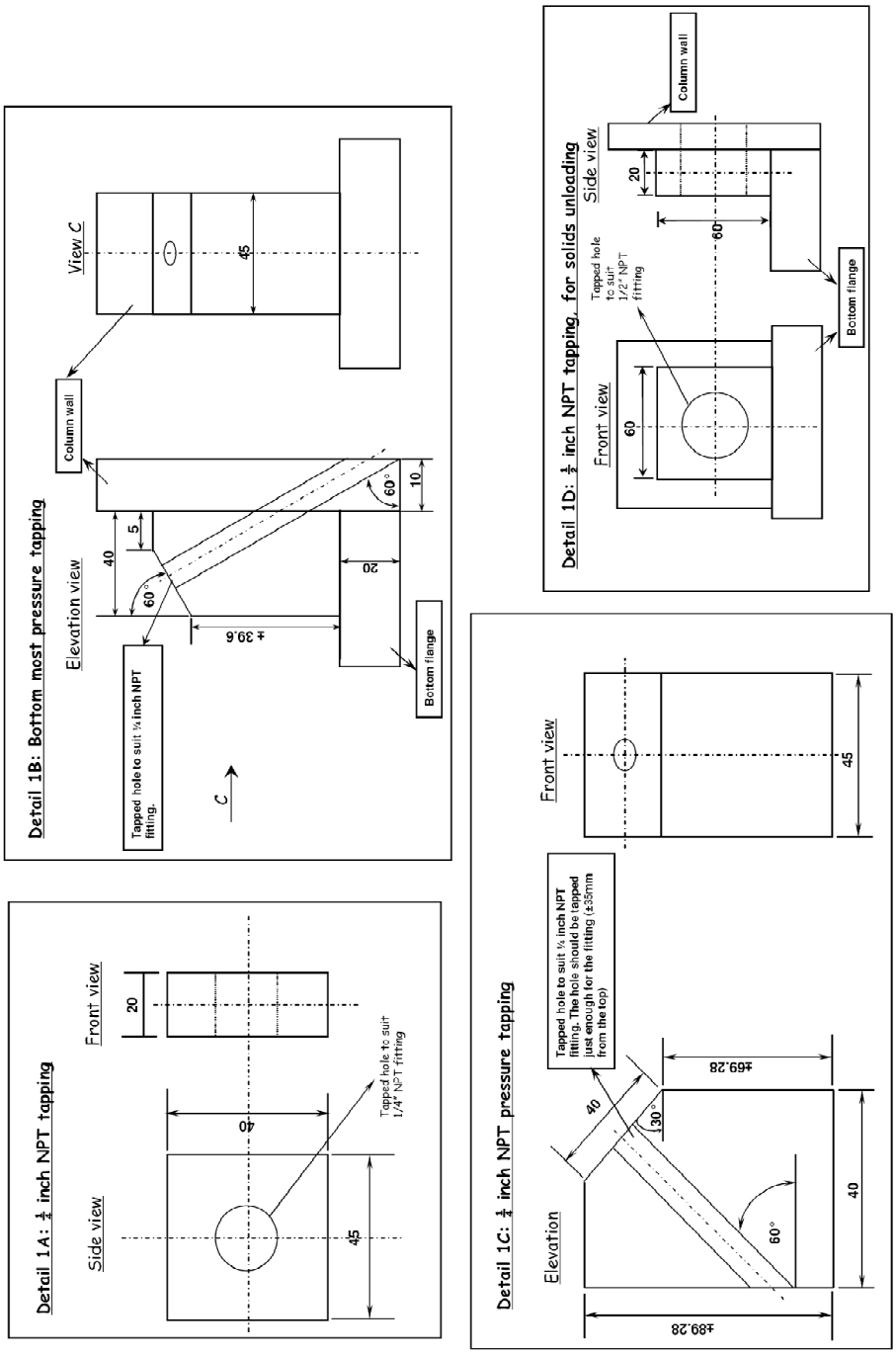
Detail 1A: ¼ inch NPT tapping
Front view
Side view
20
40
45
Tapped hole to suit 1/4" NPT fitting
Detail 1B: Bottom most pressure tapping
View C
Elevation view
Column wall
45
40
5
60°
10
20
± 39.6
Tapped hole to suit ¼ inch NPT fitting.
Bottom flange
C
Detail 1C: ¼ inch NPT pressure tapping
Front view
Elevation
Tapped hole to suit ¼ inch NPT fitting. The hole should be tapped just enough for the fitting (±35mm from the top)
45
40
30°
60°
±69.28
±89.28
Detail 1D: ½ inch NPT tapping, for solids unloading
Side view
Front view
Column wall
20
60
Tapped hole to suit 1/2" NPT fitting
Bottom flange

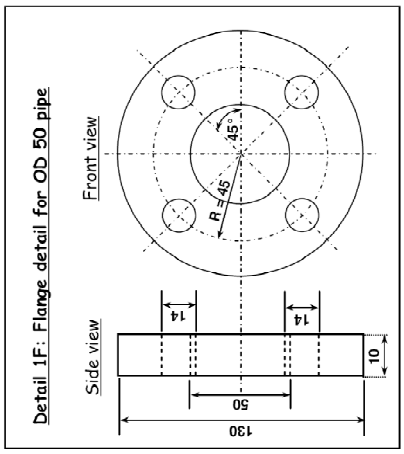
Detail 1F: Flange detail for OD 50 pipe
Front view
Side view
45°
R = 45
14
14
10
50
130

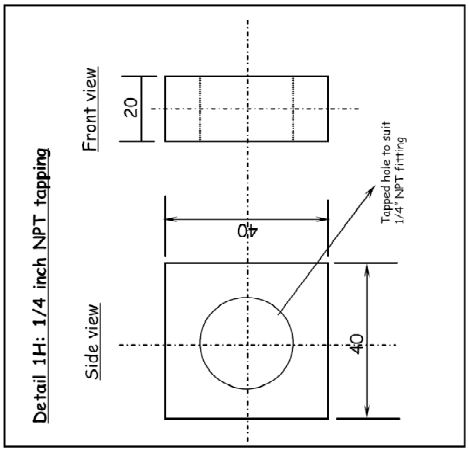
Detail 1H: 1/4 inch NPT tapping
Front view
Side view
20
40
40
Tapped hole to suit
1/4" NPT fitting

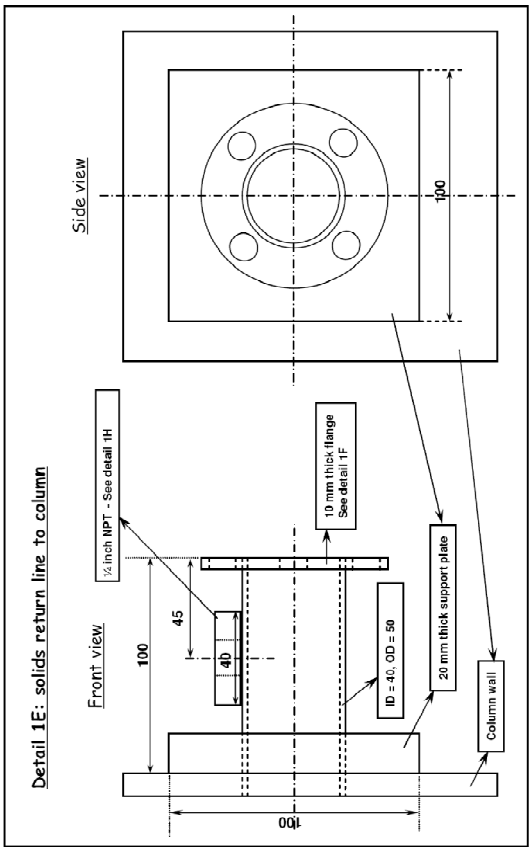
Detail 1E: solids return line to column
Front view
Side view
¼ inch NPT - See detail 1H
10 mm thick flange
See detail 1F
ID = 40, OD = 50
20 mm thick support plate
Column wall
100
45
40
100
100

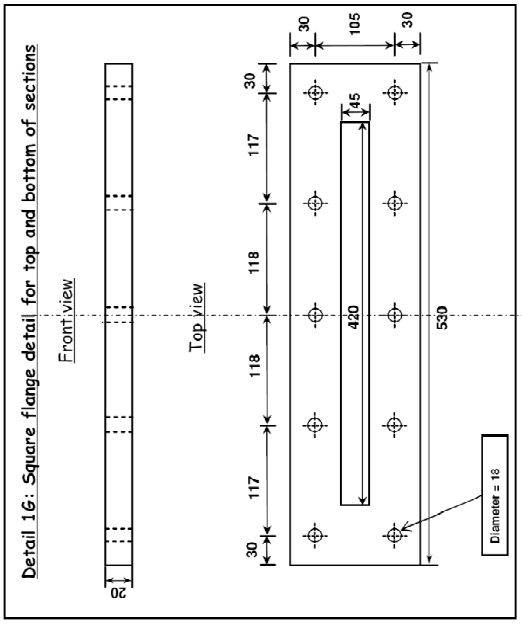
Detail 1G: Square flange detail for top and bottom of sections
Front view
Top view
20
30
105
30
30
117
118
118
117
30
45
420
530
Diameter = 18

Details for item 2

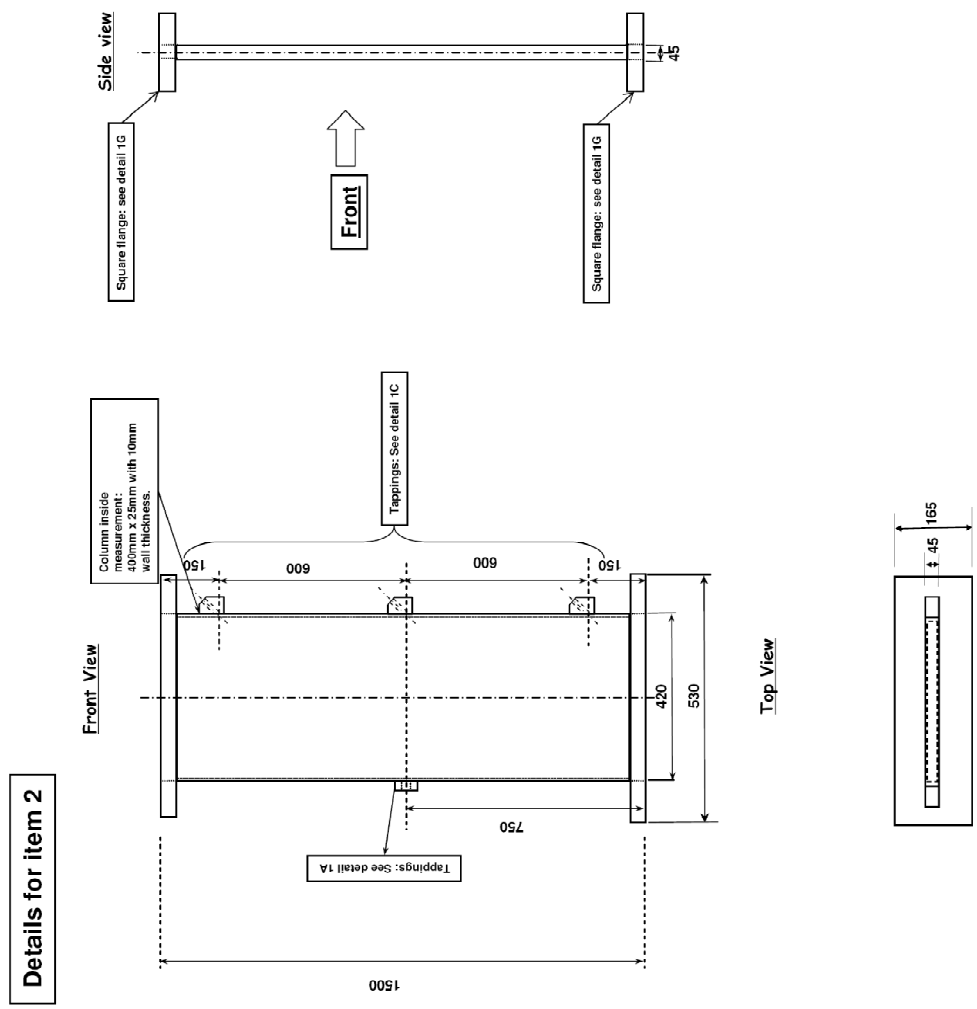

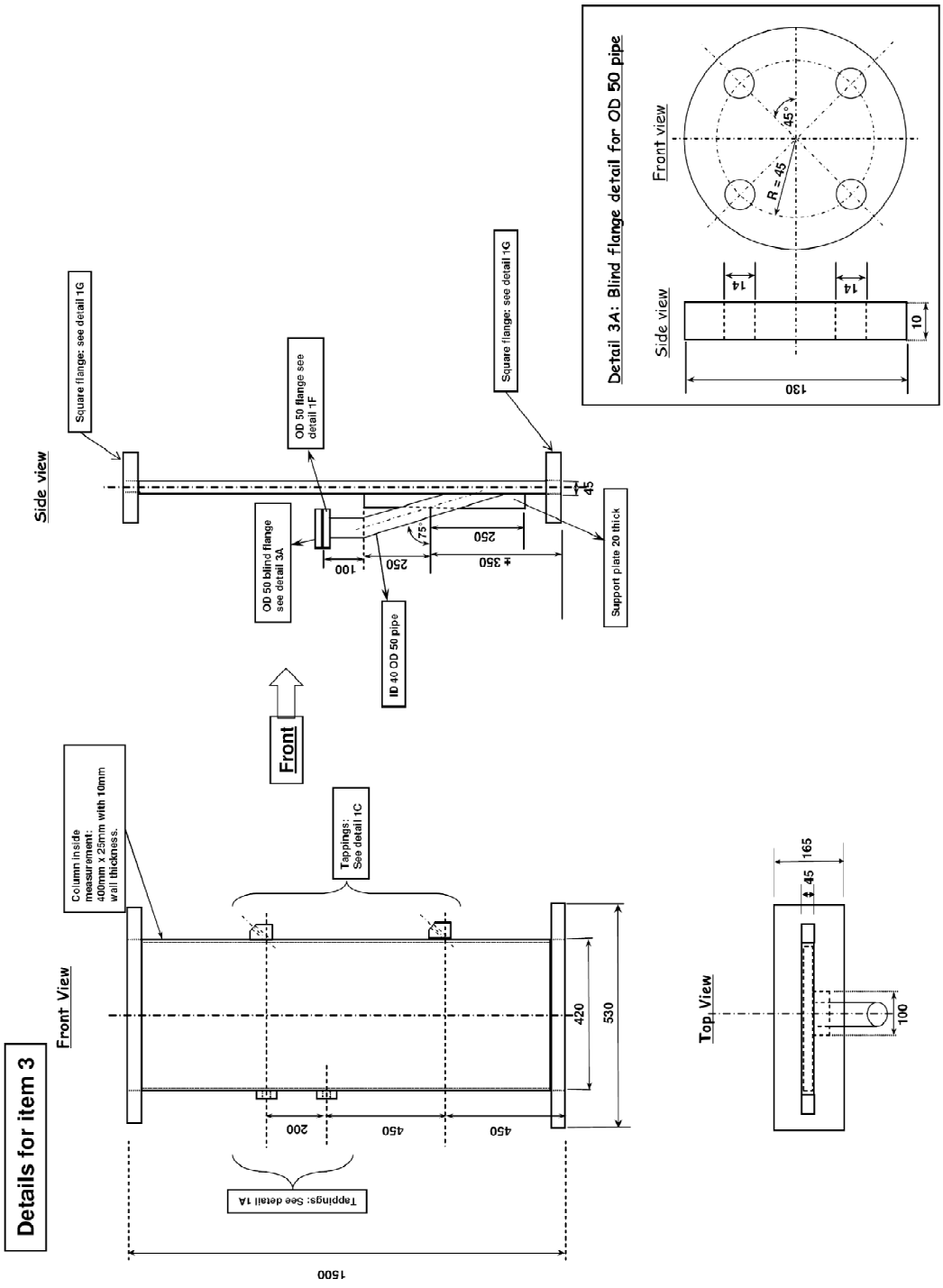
Details for item 3
Front View
Column inside measurement: 400mm x 25mm with 10mm wall thickness.
Tappings: See detail 1C
Front
Square flange: see detail 1G
OD 50 flange see detail 1F
Square flange: see detail 1G
Side view
OD 50 blind flange see detail 3A
ID 40 OD 50 pipe
Support plate 20 thick
100
250
± 350
250
75
45
Tappings: See detail 1A
200
450
450
420
530
1500
Top View
165
45
100
Detail 3A: Blind flange detail for OD 50 pipe
Front view
Side view
45°
R = 45
14
14
10
130

Details for item 4

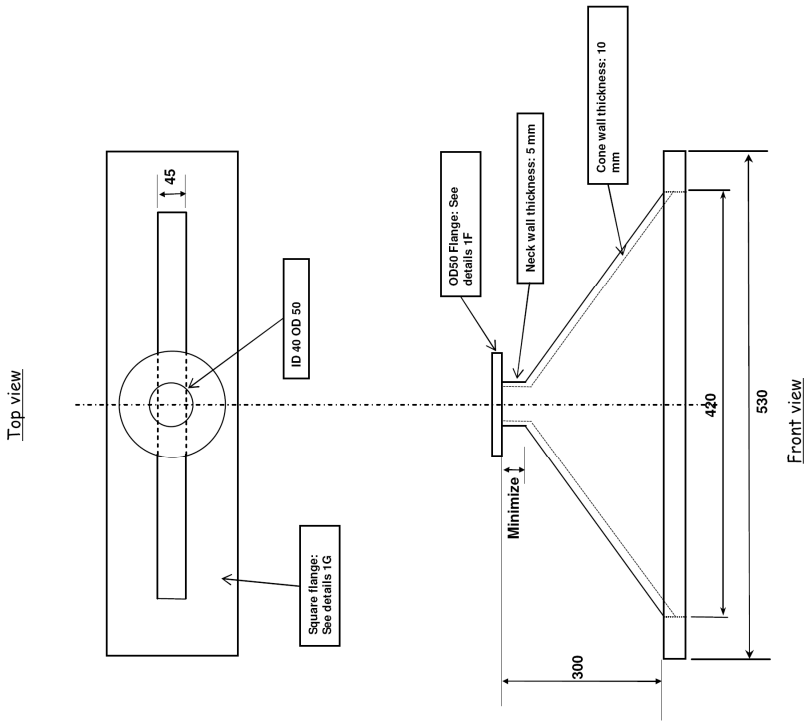

Details for item 5

Note:
1. All piping is ID = 40 and OD = 50 clear plexiglas, except for cyclones (see detail for item 6 and 7)
2. All elbows and T-pieces that are shaded should be standard PVC fittings (commercially available)
3. Plexiglas piping between elbows, T-pieces and valves and flanges should be determined so as to minimize the overall height and length of the layout shown below (unless details are specified)
4. All flanges for OD 50 - pipe see detail 1F

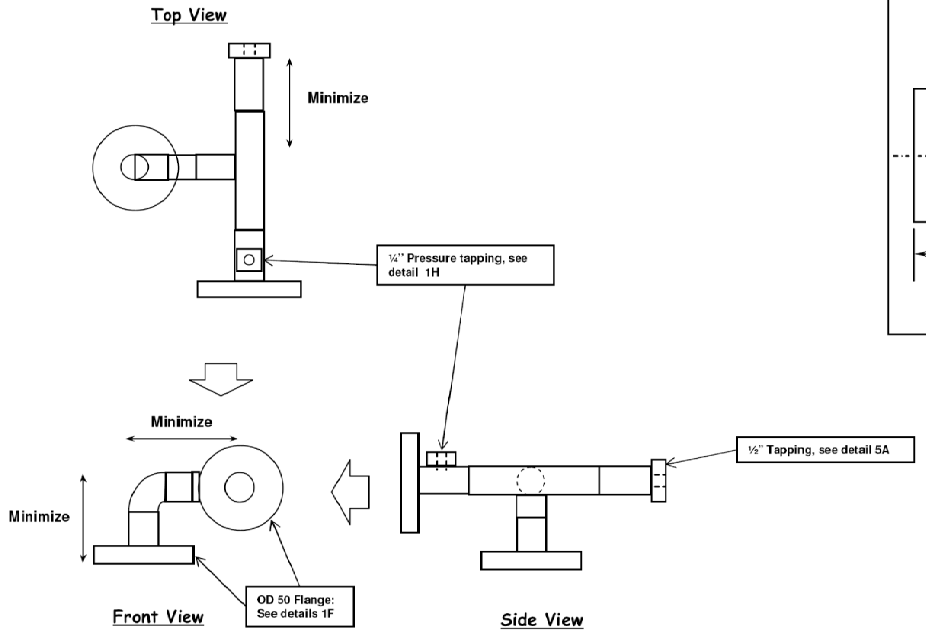

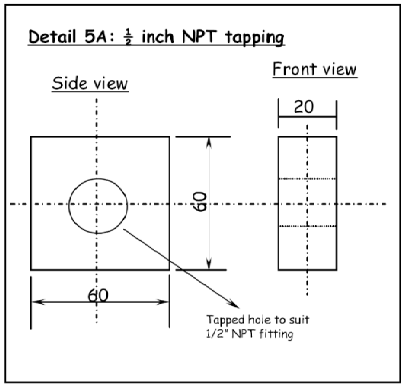

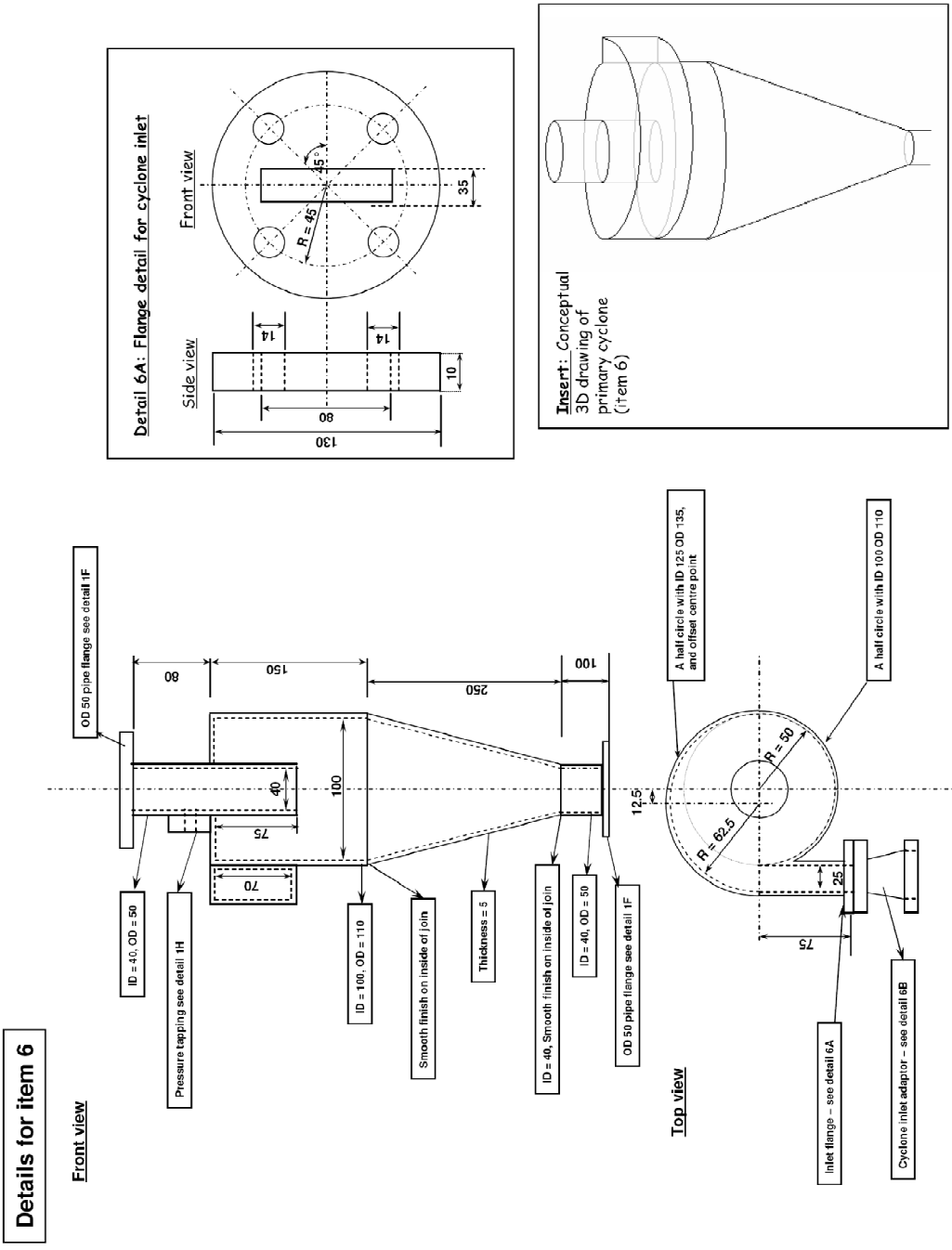
Details for item 6
Front view
OD 50 pipe flange see detail 1F
80
150
250
100
40
100
75
70
12.5
ID = 40, OD = 50
Pressure tapping see detail 1H
ID = 100, OD = 110
Smooth finish on inside of join
Thickness = 5
ID = 40, Smooth finish on inside of join
ID = 40, OD = 50
OD 50 pipe flange see detail 1F
Top view
A half circle with ID 125 OD 135, and offset centre point
A half circle with ID 100 OD 110
R = 50
R = 62.5
25
75
Inlet flange – see detail 6A
Cyclone inlet adaptor – see detail 6B
Detail 6A: Flange detail for cyclone inlet
Front view
Side view
45°
R = 45
35
14
14
10
80
130
Insert: Conceptual 3D drawing of primary cyclone (item 6)

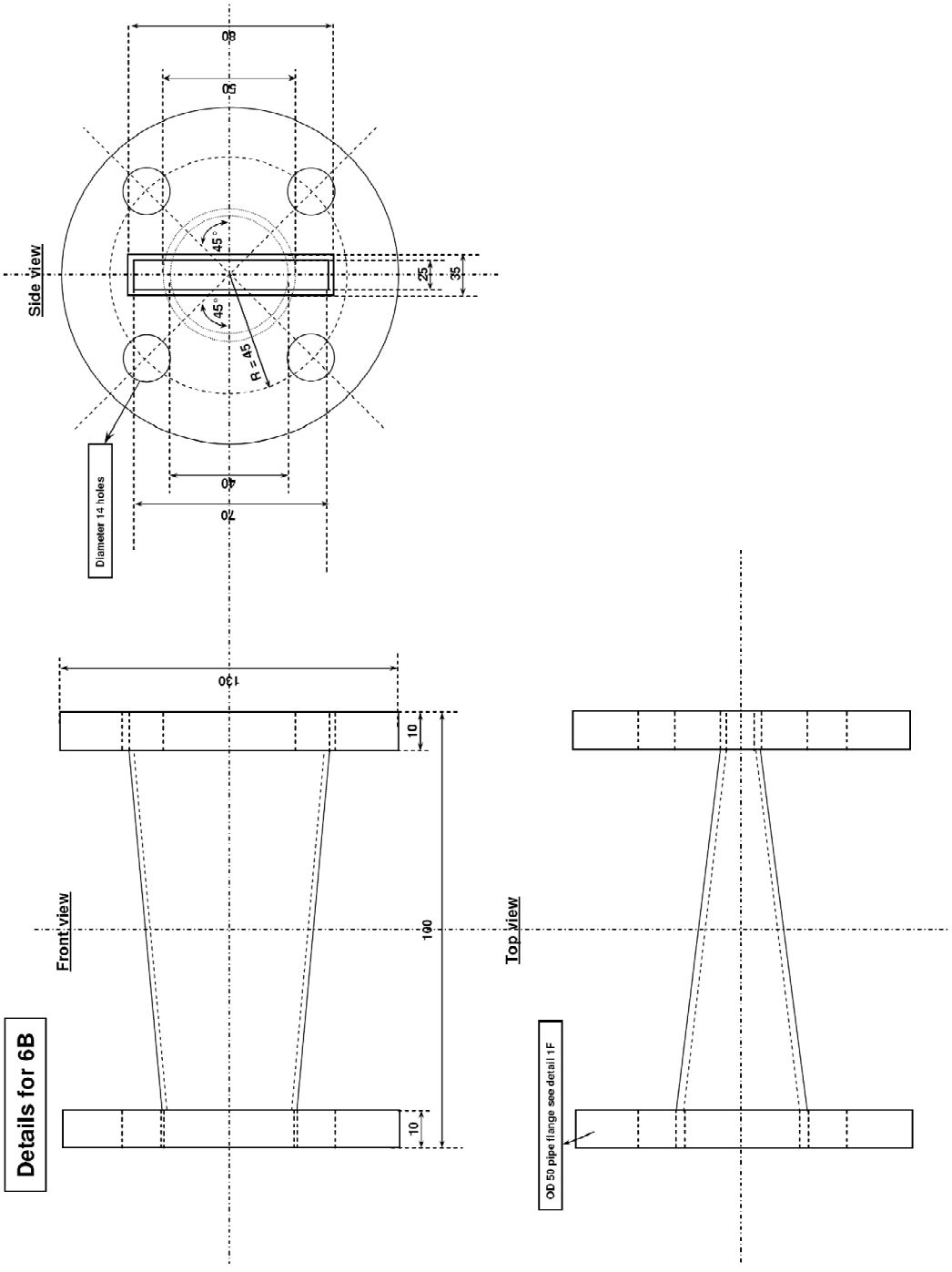
Details for 6B
Side view
Front view
Top view
Diameter 14 holes
OD 50 pipe flange see detail 1F
80
50
40
70
45°
45°
R = 45
25
35
130
10
100
10

Details for 6-2

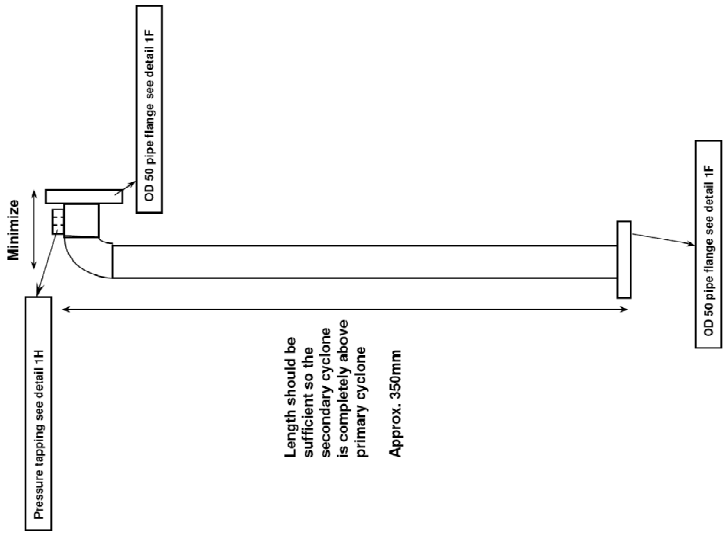

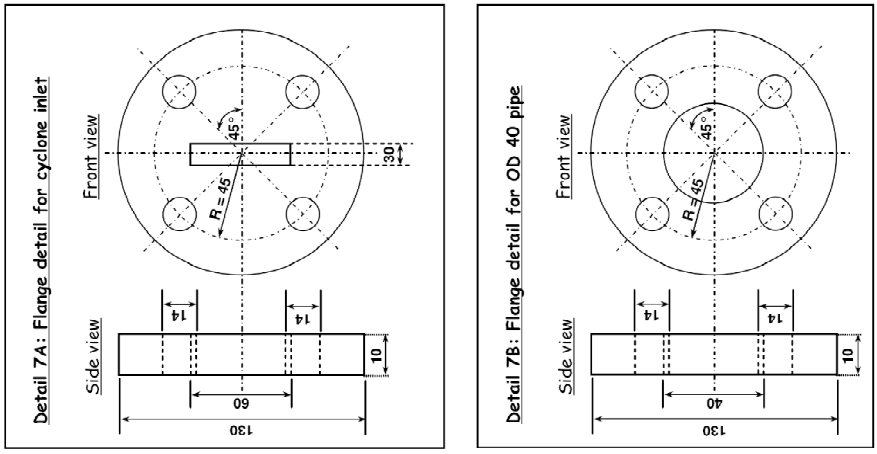
Detail 7A: Flange detail for cyclone inlet
Front view
Side view
45°
R = 45
30
14
14
10
60
130
Detail 7B: Flange detail for OD 40 pipe
Front view
Side view
45°
R = 45
14
14
10
40
130

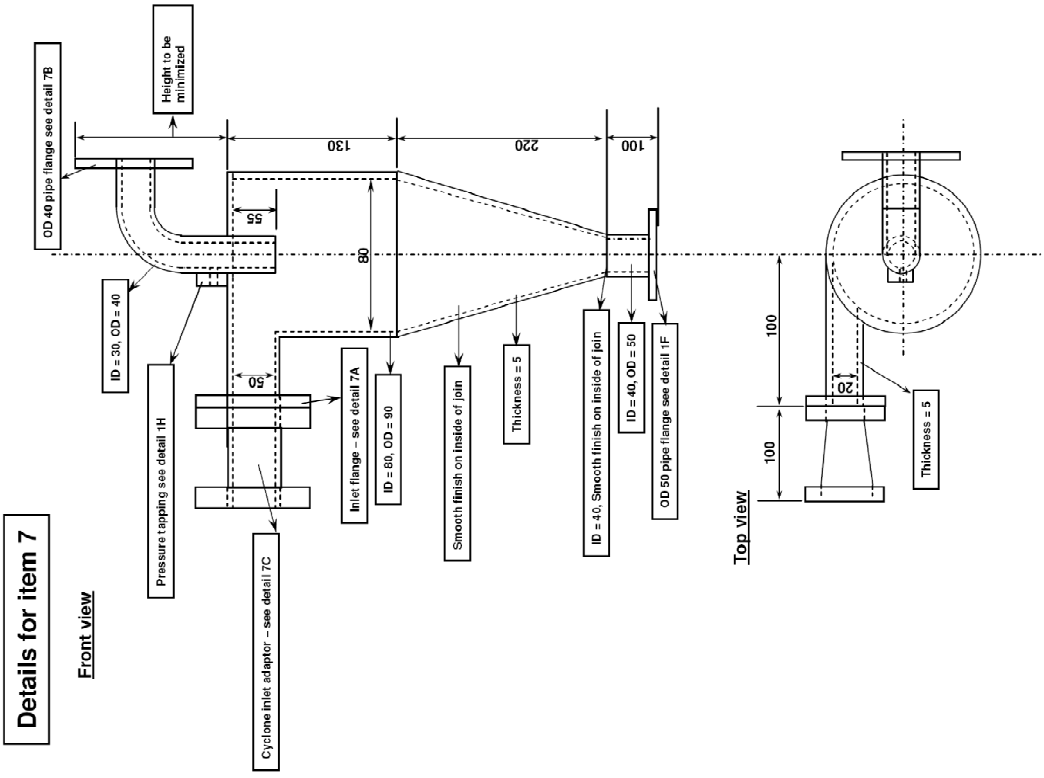
Details for item 7
Front view
OD 40 pipe flange see detail 7B
Height to be minimized
130
220
100
55
80
ID = 30, OD = 40
Pressure tapping see detail 1H
50
Cyclone inlet adaptor – see detail 7C
Inlet flange – see detail 7A
ID = 80, OD = 90
Smooth finish on inside of join
Thickness = 5
ID = 40, Smooth finish on inside of join
ID = 40, OD = 50
OD 50 pipe flange see detail 1F
Top view
100
100
20
Thickness = 5

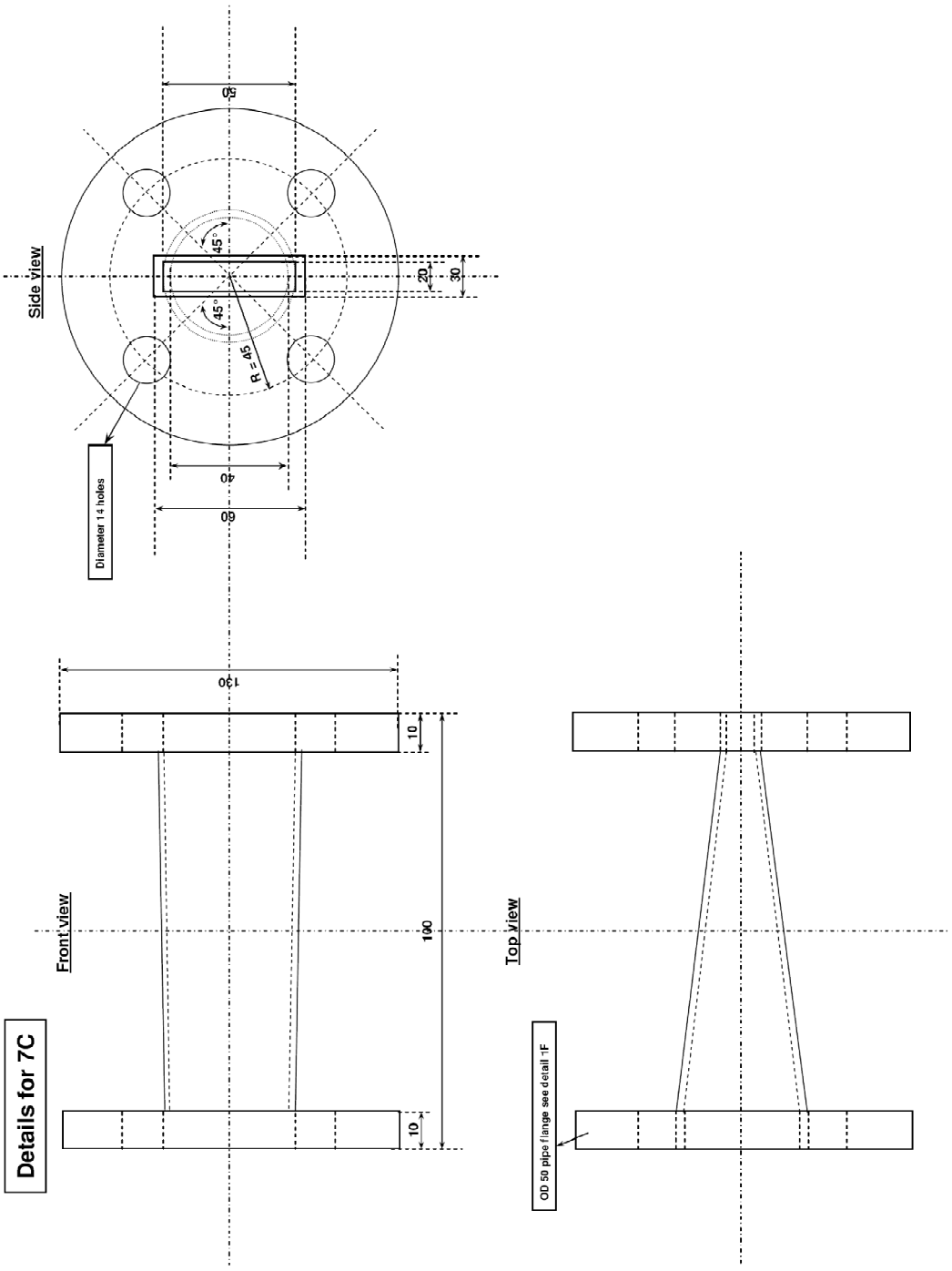
Details for 7C
Side view
Front view
Top view
50
45°
45°
20
30
R = 45
40
60
Diameter 14 holes
130
10
100
10
OD 50 pipe flange see detail 1F

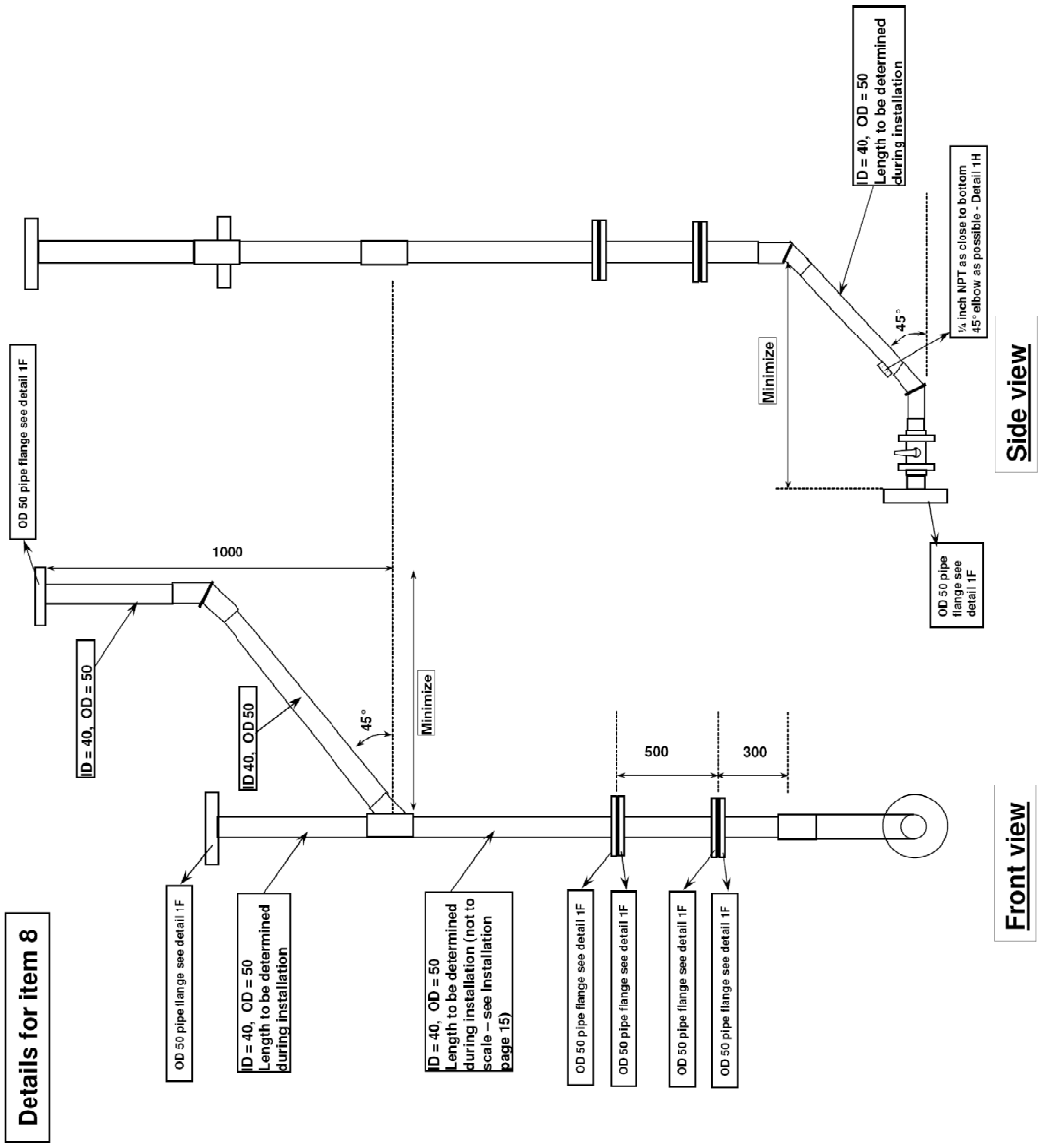
Details for item 8
OD 50 pipe flange see detail 1F
ID = 40, OD = 50
Length to be determined during installation
ID = 40, OD = 50
Length to be determined during installation (not to scale – see Installation page 15)
OD 50 pipe flange see detail 1F
OD 50 pipe flange see detail 1F
OD 50 pipe flange see detail 1F
OD 50 pipe flange see detail 1F
Front view
1000
ID = 40, OD = 50
ID 40, OD 50
45°
Minimize
500
300
OD 50 pipe flange see detail 1F
Minimize
45°
½ inch NPT as close to bottom 45° elbow as possible - Detail 1H
ID = 40, OD = 50
Length to be determined during installation
OD 50 pipe flange see detail 1F
Side view

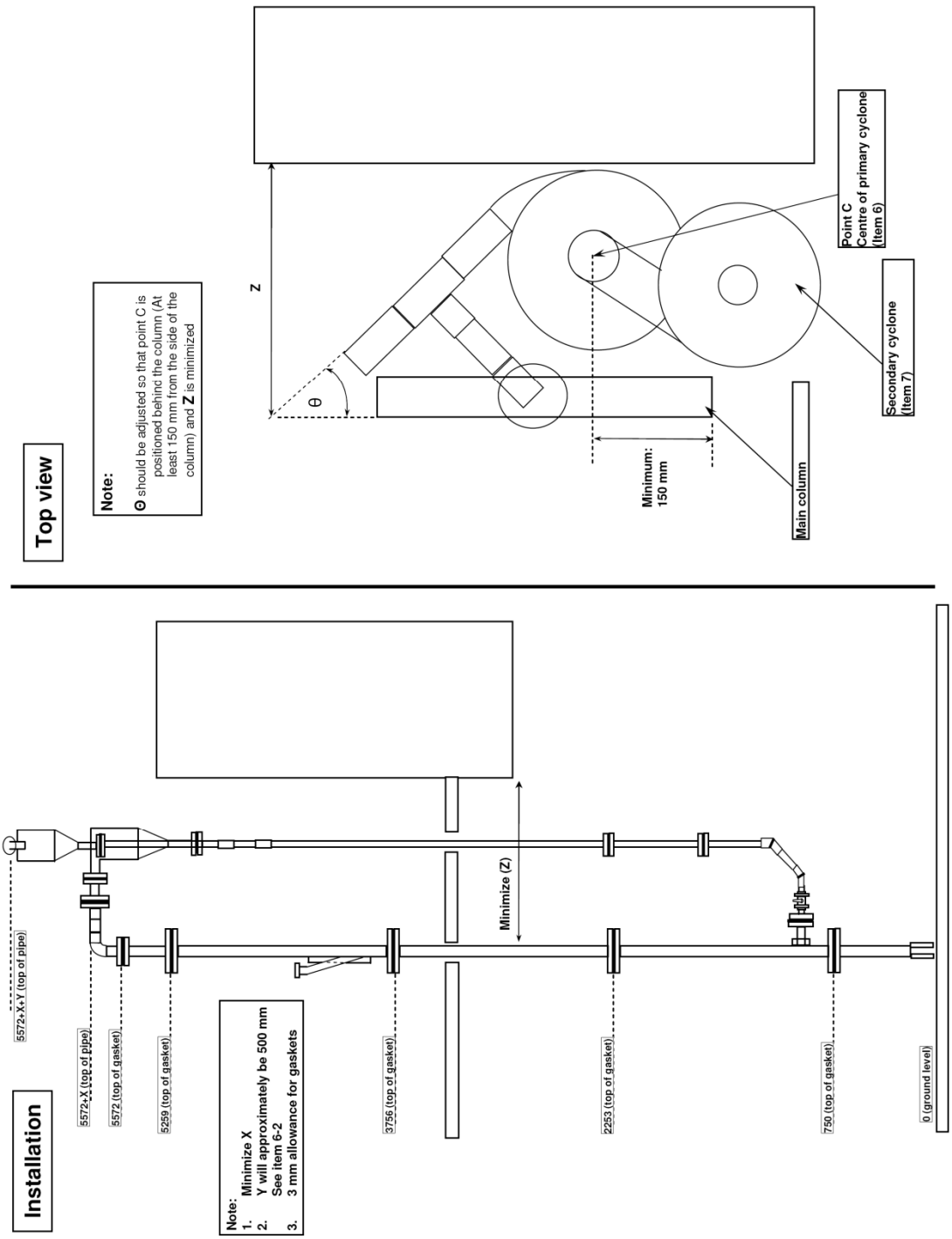
Top view
Note:
Θ should be adjusted so that point C is positioned behind the column (At least 150 mm from the side of the column) and Z is minimized
Z
θ
Point C
Centre of primary cyclone
(Item 6)
Secondary cyclone
(Item 7)
Minimum:
150 mm
Main column
Installation
5572+X+Y (top of pipe)
5572+X (top of pipe)
5572 (top of gasket)
5259 (top of gasket)
3756 (top of gasket)
2253 (top of gasket)
750 (top of gasket)
0 (ground level)
Minimize (Z)
Note:
1. Minimize X
2. Y will approximately be 500 mm
See item 6-2
3. 3 mm allowance for gaskets

Item 9 – Made of Metal and not Perspex

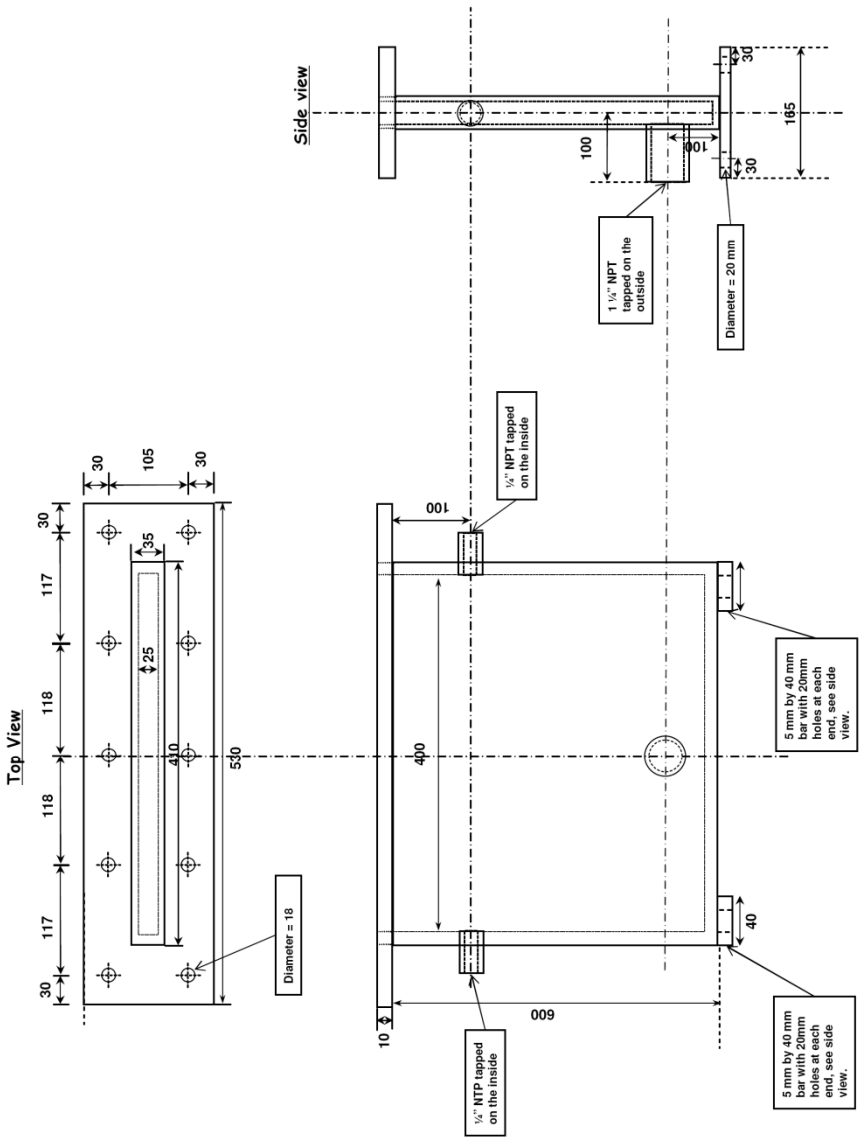

Appendix B: Reaction rate results for improving catalyst activity

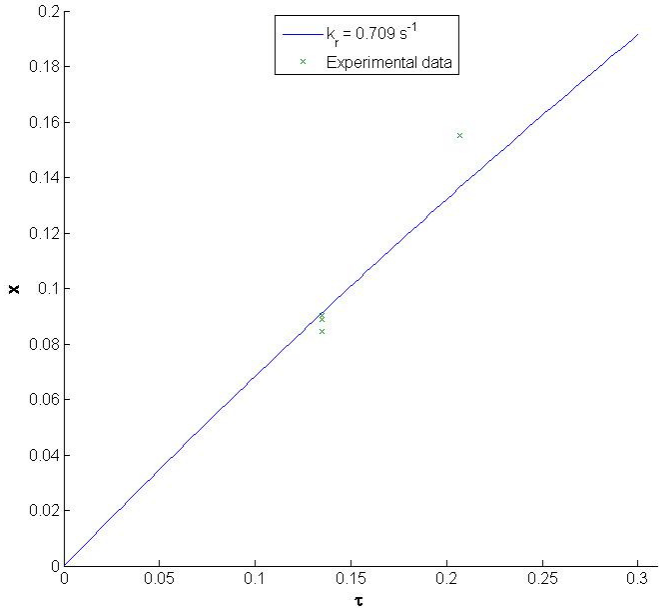

Figure B.1: Catalyst prepared in 10 %(wt) Ferric Nitrate Solution, soaked for 1 hour, calcinated at 450 ˚C for 1.4 hours. $k_r = 0.71\ s^{-1}$.

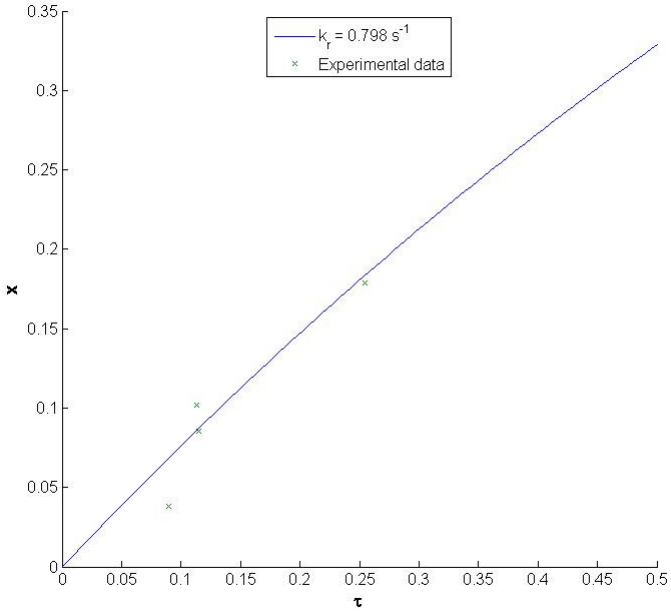

Figure B.2: Catalyst prepared in 5 %(wt) Ferric Nitrate Solution, soaked for 12 hour, calcinated at 450 ˚C for 1.4 hours. $k_r = 0.80\ s^{-1}$.

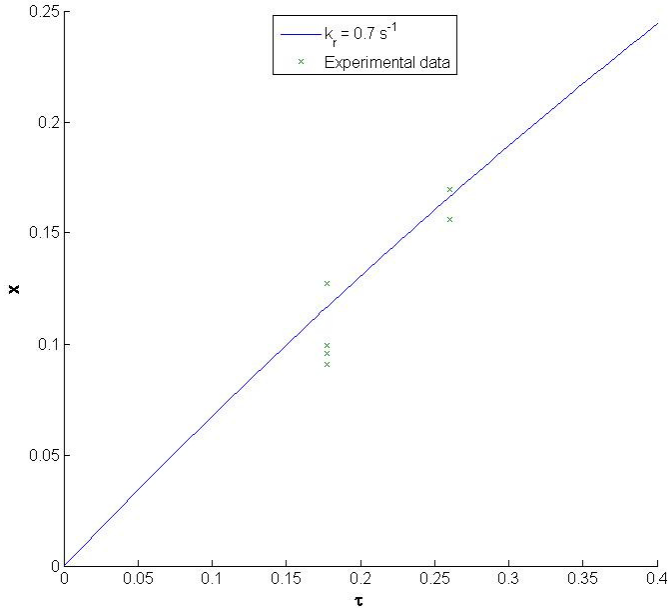

Figure B.3: Catalyst prepared in 5 %(wt) Ferric Nitrate Solution, soaked for 1 hour, calcinated at 500 ˚C for 1.4 hours. $k_r = 0.70\ s^{-1}$.

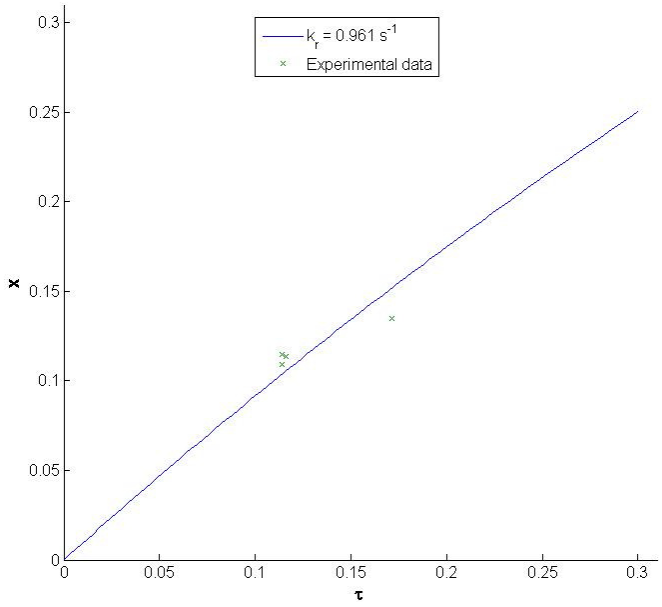

Figure B.4: Catalyst prepared in 5 %(wt) Ferric Nitrate Solution, soaked for 1 hour, calcinated at 475 ˚C for 2 hours. $k_r = 0.96\ s^{-1}$.